Journal of Constructional Steel Research 65 (2009) 1876–1895

Contents lists available at ScienceDirect

Journal of Constructional Steel Research

journal homepage: www.elsevier.com/locate/jcsr

Generalised component-based model for beam-to-column connections including axial versus moment interaction

A.A. Del Savio [a,b,*], D.A. Nethercot [b,1], P.C.G.S. Vellasco [c,2], S.A.L. Andrade [c,a], L.F. Martha [a,3]

[a] Civil Engineering Department, PUC-Rio – Pontifical Catholic University of Rio de Janeiro, Rua Marquês de São Vicente, 225, Gávea, CEP: 22453-900, Rio de Janeiro, RJ, Brazil

[b] Department of Civil and Environmental Engineering, Imperial College London, South Kensington Campus, Skempton Building, London SW7 2BU, United Kingdom

[c] Structural Engineering Department, UERJ – State University of Rio de Janeiro, Rua São Francisco Xavier, 524, Sala 5018A, Maracanã, CEP: 20550-900, Rio de Janeiro, RJ, Brazil

ARTICLE INFO

Article history:
Received 13 November 2007
Accepted 27 February 2009

Keywords:
Steel structures
Semi-rigid joints
Joint behaviour
Axial versus bending moment interaction
Mechanical model
Component method
Rotational stiffness

ABSTRACT

A generalised component-based model for semi-rigid beam-to-column connections including axial force versus bending moment interaction is presented. The detailed formulation of the proposed analytical model is fully described in this paper, as well as all the analytical expressions used to evaluate the model properties. Detailed examples demonstrate how to use this model to predict moment–rotation curves for any axial force level. Numerical results, validated against experimental data, form the basis of a tri-linear approach to characterise the force–displacement relationship of the joint components. The relationship of the present development to key prior studies of this topic is also explained.

1. Introduction

The continuous search for the most accurate representation of structural behaviour depends directly on detailed structural modelling, including the interactions between all the structural elements, linked to the overall structural analysis procedures, such as material and geometric non-linear analysis. This strategy permits a more realistic modelling of connections, instead of the usual pinned or rigid assumptions. This idea is crucial to advance towards a better overall structural behavioural understanding, since joint response is well-described by the moment–rotation curve. However, this approach requires a complete knowledge of semi-rigid joint behaviour, which is, for some situations, beyond the scope of present knowledge e.g. the influence of axial forces on the joint bending moment versus the rotation characteristic. In addition to permitting the most accurate structural modelling, the use of semi-rigid joints has several practical advantages such as those identified in [1]: economy of both design effort and fabrication costs; beams may be lighter than in simple constructions; reduction of mid-span deflection due to the inherent stiffness of the joint; connections are less complicated than in continuous construction; frames are more robust than in simple construction; and for an unbraced frame, additional benefits may be gained from semi-continuous joints in resisting wind loading without the extra fabrication costs incurred when full continuity is adopted.

Under certain circumstances, beam-to-column joints can be subjected to the simultaneous action of bending moments and axial forces. Although the axial force transferred from the beam is usually low, it may, in some situations attain values that significantly reduce the joint flexural capacity. These conditions may be found in: structures under fire situations where the effects of beam thermal expansion and membrane action can induce significant axial forces in the connection [2]; Vierendeel girder systems (widely used in building construction because they take advantage of the member flexural and compression resistances eliminating the need for extra diagonal members); regular sway frames under significant horizontal loading (seismic or extreme wind); irregular frames (especially with incomplete storeys) under gravity/horizontal loading; and pitched-roof frames. In addition, due to the recent escalation of terrorist attacks on buildings, the investigation of progressive collapse of steel framed buildings has been highlighted, as can be seen in [3]. Examples of these exceptional conditions are the cases where structural elements,

* Corresponding author at: Civil Engineering Department, PUC-Rio – Pontifical Catholic University of Rio de Janeiro, Rua Marquês de São Vicente, 225, Gávea, CEP: 22453-900, Rio de Janeiro, RJ, Brazil. Tel.: +55 21 3527 1188; fax: +55 21 3527 1195.
E-mail addresses: delsavio@gmail.com (A.A. Del Savio), d.nethercot@imperial.ac.uk (D.A. Nethercot), vellasco@eng.uerj.br (P.C.G.S. Vellasco), andrade@civ.puc-rio.br (S.A.L. Andrade), lfm@tecgraf.puc-rio.br (L.F. Martha).

[1] Tel.: +44 20 7594 6097; fax: +44 20 7594 6049.

[2] Tel.: +55 21 2587 7537; fax: +55 21 2587 7537.

[3] Tel.: +55 21 35 27 1188; fax: +55 21 35 27 1195.

0143-974X/$ – see front matter © 2009 Elsevier Ltd. All rights reserved.
doi:10.1016/j.jcsr.2009.02.011

Nomenclature

l_i	distance from joint spring/row i to the beam bottom flange centre
b_1	model first bar representing the beam end
b_2	model second bar representing the column flange centreline
bfwc	beam flange and web in compression
bt	bolts in tension
bwt	beam web in tension
cfb	column flange in bending
cwc	column web in compression
cws	column web in shear
cwt	column web in tension
d	lever arm: distance from the loading application centre to the rigid link
d_i	system displacements, $i = 1 \ldots 4$: $u_{b1}, \theta_{b1}, u_{b2}, \theta_{b2}$
e	distance from the loading application centre to the beam bottom flange
epb	endplate in bending
$f^y_{br,i}$	yield strength of the joint bolt-row i
f^y_{cp}	joint component yield capacity
f^u_{cp}	joint component ultimate capacity
f_i	force in spring/row i
f^y_i	yield capacity of spring/row i
f^u_i	ultimate capacity of spring/row i
r_i	tangent effective stiffness of spring/row i
k_{bbf}	elastic stiffness of the beam bottom flange
$k_{br1,2,3}$	elastic stiffness of bolt-rows 1, 2 and 3 respectively
k_{btf}	elastic stiffness of the beam top flange
k^e_{cp}	joint component elastic stiffness
k^p_{cp}	joint component plastic stiffness
k^u_{cp}	joint component reduced strain hardening stiffness
k_{lcbf}	compressive link elastic stiffness associated with the beam bottom flange
k_{lctf}	compressive link elastic stiffness associated with the beam top flange
k_{lt}	tensile link elastic stiffness associated with the lever arm
$k_{lt1,2,3}$	tensile link elastic stiffness associated with the bolt-rows 1, 2 and 3, respectively
r^e_i	elastic effective stiffness of spring/row i
r^p_i	plastic effective stiffness of spring/row i
r^u_i	reduced strain hardening effective stiffness of spring/row i
nbr	number of joint bolt-rows
nc	row/spring component number
ns	model spring/row number
ns_{b1}	spring/row number between the model first and second bars
u_{b1}	first bar displacement
u_{b2}	second bar displacement
u_i	absolute displacement of spring/row i (first bar)
ul_i	absolute displacement of spring/row i (second bar)

Capital letter

C_i	spring/row i vertical coordinates
F	internal loading vector
F_i	terms of the internal loading vector, $i = 1 \ldots 4$
F_{bbf}	row compressive yield capacity (beam bottom flange)
F_{linkt}	rigid link tensile capacity, which joins the second bar to the supports
F_{Rd}	joint component design strength
K	model/joint stiffness matrix
K^e	joint elastic stiffness
K^p	joint plastic stiffness
K^u	joint ultimate stiffness
K_{ij}	terms of the model stiffness matrix, $i = 1 \ldots 4$ and $j = 1 \ldots 4$
M	bending moment applied to the connection
M^f	bending moment referred to a 0.05-rad joint final rotation
M^u	bending moment that leads the joint to failure
M^y	bending moment that leads the joint to yielding
$M^u_{br,i}$	bending moment that leads to failure of the joint spring/row i, located between the first and second bars
$M^y_{br,i}$	bending moment that leads to yielding of the joint spring/row i, located between the first and second bars
$M^u_{fr,i}$	bending moment that leads to failure of the joint spring/row i, located between the second bar and supports
$M^y_{fr,i}$	bending moment that leads to yielding of the joint spring/row i, located between the second bar and supports
$M_{j,\mathrm{lim}}$	limit bending moment of spring/row j, located between the first and second bars
N	axial force applied to the joint
N_{pl}	axial plastic capacity of the beam
P	axial load applied to the connection
U	system strain energy
W	load total potential

Greek letters

$\alpha_{1,2,3,4}$	coefficients of Eq. (41)
$\eta_{1,2,3,4}$	coefficients of Eq. (41)
θ	joint rotation
θ^u	joint rotation capacity necessary to develop the joint plastic bending moment
θ^y	joint rotation capacity necessary to develop the joint yield bending moment
θ^f	joint final rotation (assumed to be equal to 0.05 rad)
θ_{b1}	first bar rotation
θ_{b2}	second bar rotation
κ	stiffness coefficient (Eq. (18))
λ	stiffness coefficient (Eq. (18))
μ^p	plastic stiffness strain hardening coefficient
μ^u	ultimate stiffness strain hardening coefficient
ξ	stiffness coefficient (Eq. (23))
ρ	stiffness coefficient (Eq. (18))
υ	stiffness coefficient (Eq. (26))
φ	stiffness coefficient (Eq. (27))
χ_1	stiffness coefficient (Eq. (23))
χ_2	stiffness coefficient (Eq. (20))
ψ	stiffness coefficient (Eq. (20))
ω_1	stiffness coefficient (Eq. (23))
ω_2	stiffness coefficient (Eq. (20))

Capital letter

Δ_i	spring/row i relative displacement

$\Delta_{br,i}$	spring/row i relative displacement located between the first and second bars
$\Delta_{fr,i}$	spring/row i relative displacement located between the second bar and the supports
Δ_i^y	relative displacement that leads to yielding of the model spring/row i
Δ_i^u	relative displacement that leads to failure of the model spring/row i
Z	stiffness coefficient (Eq. (25))
Π	total potential energy functional
X	stiffness coefficient (Eq. (22))
Ω	stiffness coefficient (Eq. (22))

such as central and/or peripheral columns and/or main beams, are suddenly removed, abruptly increasing the joint axial forces. In these situations the structural system, mainly the connections, should be sufficiently robust to prevent the premature failure modes that may lead to a progressive structural collapse.

Unfortunately, few experiments considering the bending moment versus axial force interactions have been reported. Additionally, the available experiments are related to a small number of axial force levels and associated bending moment versus rotation curves. Recently, some mechanical models have been developed, see Section 1.2, to deal with the bending moment-axial force interaction. However these models are still not able to accurately predict the joint moment–rotation curves, thereby restricting their incorporation in full analysis procedures. There is, therefore, a need to develop the mechanical model for semi-rigid beam-to-column joints including the axial force versus bending moment interaction, based on the principles of the component method, Eurocode 3 [4]. The next sections present a detailed formulation of this generalised mechanical model including a proposal for joint component characterisation, as well as examples of its application and validation against experimental tests. However, in order to fully set the scene for these developments a bibliographical review containing a brief description of the most important available techniques to predict joint structural behaviour and the most important laboratory tests is presented.

1.1. Component method

The component method entails the use of relatively simple joint mechanical models, based on a set of rigid links and spring components. The component method – introduced in [4] – can be used to determine the joint's resistance and initial stiffness. Its application requires the identification of active components, the evaluation of the force–deformation response of each component (which depends on mechanical and geometrical properties of the joint) and the subsequent assembly of the active components for the evaluation of the joint moment versus rotation response.

Nowadays, using the Eurocode 3 [4] component method, it is possible to evaluate the rotational stiffness and moment capacity of semi-rigid joints when subject to pure bending. However, this component method is not yet able to calculate these properties when, in addition to the applied moment, an axial force is also present. Eurocode 3 [4] suggests that the axial load may be disregarded in the analysis when its value is less than 5% of the beam's axial plastic resistance, but provides no information for cases involving larger axial forces. Although the component method does not consider the axial force, its general principles could be used to cover this situation, since it is based on the use of a series of force versus displacement relationships, which only depend on the component's axial force level, to characterise any individual component's behaviour.

1.2. Background

The study of the semi-rigid characteristics of beam to column connections and their effects on frame behaviour can be traced back to the 1930s, [5]. Since then, a large amount of experimental and theoretical work has been conducted both on the behaviour of the connections and on their effects on complete frame performance. Despite the large number of experiments, few of them consider the bending moment versus axial force interactions.

This section has attempted to provide a summary of the techniques currently available to predict the joint structural behaviour, as well as a brief discussion of some experimental tests, focusing on the study of joint behaviour under combined bending moment and axial force using mechanical models.

1.2.1. Experimental

A detailed discussion of all available experimental tests is beyond the scope of this paper; a compilation of the experiments is, however, available in [6]; [7, SERICON I] and [8, SERICON II]. Recently, several researchers have paid special attention to joint behaviour under combined bending moment and axial force. Guisse et al. [9] carried out experiments on twelve column bases, six with extended and six with flush endplates. Wald and Svarc [10] tested three flush endplate beam-to-beam joints and two extended endplate beam-to-column joints; however there is no reference to tests made with only bending moment, which is vital to access the influence of the axial force in the joint response. Lima et al. [11] and Simões da Silva et al. [12] performed tests on eight flush endplate joints and seven extended endplate joints. The investigators concluded that the presence of the axial force in the joints modifies their structural response and should, therefore, be considered in the joint structural design.

1.2.2. Theoretical models

As an alternative to tests, other methods have been proposed to predict bending moment versus rotation curves. These procedures range from a purely empirical curve fitting of test data, passing through ingenious behavioural, analogy and semi-empirical techniques, to comprehensive finite element analysis, [13].

1.2.2.1. Mathematical formulations (empirical models). The first attempt at fitting a mathematical representation to connection moment–rotation curves dates back to the work of Baker [14] and Rathbun [15], who used a single straight-line tangent to the initial slope, thereby overestimating connection stiffness at finite rotations. In the 1970s the use of bilinear representations was introduced by Lionberger & Weaver [16] and Romstad & Subramanian [17]. These recognised the reduced stiffness at higher rotations, however it was only acceptable for certain joint types and for applications where only small joint rotations are likely. Kennedy [18], Sommer [19] and Frye & Morris [20] proposed polynomial representations that recognised the curved nature, but required mathematical curve fitting and consideration of a family of experimental moment–rotation curves. Ang & Morris [21] replaced the polynomial representation by a Ramberg & Osgood [22] type of exponential function that has the advantage of always yielding a positive slope, but is also dependent on mathematical curve fitting. Multi-linear representations were proposed by Moncarz & Gerstle [23] and Poggi & Zandonini [24] to overcome the obvious limitation of the bilinear model in that it could not deal with continuous changes in stiffness in the knee region. B-spline techniques were suggested by Jones et al. [25] as an alternative to polynomials as a means of avoiding possible negative slopes. Lui & Chen [26] used an exponential representation that despite being complex could readily be incorporated in analytical computer programmes [27]. Although it is possible to closely fit virtually

any shape of moment–rotation curve, purely empirical methods possess the disadvantage that they cannot be extended outside the range of the calibration data. This is particularly important for joints such as endplates where the change in geometrical and mechanical properties of the connection may lead to substantially different behaviours and collapse mechanisms [13]. Aiming to overcome this limitation, Yee & Melchers [28], Kishi et al. [29, 30] and Chen & Kishi [31] proposed models linking curve fitting approaches to some form of behavioural model, but these were still dependent on a mathematical curve fitting.

Focusing on finite element analysis, Richard et al. [32] used a type of formula already developed by Richard & Abbott [33] to represent data generated by finite element analyses in which the constitutive relations of certain of the joint components, e.g. bolts in shear, were directly obtained from subsidiary tests.

Each of the models discussed so far may only be used to describe the joint behaviour under a single application of a monotonically increasing load. However, some of them were modified and/or adapted to represent the performance of certain connection types under cyclic loading, as can be seen in the work done by Moncarz & Gerstle [23], Altman et al. [34] and Mazzolani [35].

Aiming to incorporate a limited set of experiments including the axial versus bending moment interaction into a structural analysis, Del Savio et al. [36] developed a consistent and simple approach to determine moment–rotation curves for any axial force level. Basically, this method works by finding moment–rotation curves through interpolations executed between three required moment–rotation curves, one disregarding the axial force effect and two considering the compressive and tensile axial force effects. This approach can be easily incorporated into a nonlinear joint finite element formulation since it does not change the finite element basic formulation, only requiring a rotational stiffness update procedure.

1.2.2.2. Simplified analytical models. Several authors have applied the basic concepts of structural analysis (equilibrium, compatibility and material constitutive relations) to simplified models of the key components in various types of beam-to-column connections [13]. Lewitt et al. [37] provided formulae for the load–deformation behaviour of double web cleat connections in both the initial and the final plastic phases; however these models needed to be used in conjunction with knowledge of the connection rotation centre. Chen & Kishi [31] and Kishi et al. [29,30] considered the behaviour of web cleats, flange cleats and combined web and flange cleat connections where their resulting values of initial connection stiffness and ultimate moment capacity were utilised in a Richard type of power expression [33] to represent the resulting moment–rotation curve. Assuming that the behaviour of the whole joint may be obtained simply by superimposing the flexibilities of the joint components (member elements, connecting, elements, fasteners) Johnson & Law [38] proposed a method for the prediction of the initial stiffness and plastic moment capacity of flush endplate connections, however no comparison was conducted against experimental results. Based on the same philosophy, Yee & Melchers [28] developed a method for bolted endplate eave connections in which an exponential representation was assumed, which depends on four parameters where only one is dependent on test data. Richard et al. [39] proposed a four-parameter formula to describe the load–deformation and moment–rotation relationship for bolted double framing angle connections. This model is composed of a rigid bar and a nonlinear spring, representing the angle segments in either tension or compression. The moment–rotation behaviour of the connections is determined through an iterative procedure by satisfying equilibrium and compatibility conditions. A similar approach was developed and used by Elsati & Richard [40] in a computer-based programme to validate the model against the test results of a variety of connection types for both composite and steel beam connections. A three-parameter exponential model was suggested by Wu & Chen [41] to model top and seat angles with and without double web angle connection and due to its simplicity it could be implemented in the analysis of semi-rigid frames. In the same year, Kishi & Chen [42] proposed a semi-analytical model to predict moment–rotation curves of angle connections, which later was extended by Foley & Vinnakota [43] for unstiffened extended endplate connections. Although these methods require a few key parameters, the use of test data is normally necessary to calibrate some of their coefficients. A wider discussion about some of these methods can be found in [13,44].

1.2.2.3. Finite element analysis. Numerical simulation started being used as a way to overcome the lack of experimental results; to understand important local effects that are difficult to measure with sufficient accuracy, e.g. prying forces and extension of the contact zone, contact forces between the bolt and the connection components; and to generate extensive parametric studies. The first study into joint behaviour making use of the FEM was executed by Bose et al. [45] related to welded beam-to-column connections, where an incremental analysis was performed, including in the formulation plasticity, with strain hardening, and buckling. The comparison with available experimental results showed satisfactory agreement, but only the critical load levels were considered. Since then, several researchers have been using the FEM to investigate joint behaviour, such as: Lipson & Hague [46] — single-angle bolted-welded connection; Krishnamurthy et al. [47] — extended endplate connections; Richard et al. [48] — double-angle connection; Patel & Chen [49] — welded two-side connections; Patel & Chen [50] — bolted moment connection; Kukreti et al. [51] — flush endplate connections; Beaulieu & Picard [52] — bolted moment connection; Atamiaz Sibai & Frey [53] — welded one-side unstiffened joint configuration. More recently, focusing on 3D finite element models the following works can be mentioned: Sherbourne & Bahaari [54], Bursi & Jaspart [55,56], Yang et al. [57], Cardoso [58], Citipitioglu et al. [59], Coelho et al. [60], and Maggi et al. [61].

1.2.2.4. Mechanical models (component-based approaches). Mechanical models have been developed by several researchers for the prediction of moment–rotation curves for the whole range of connections/joints, where the number of physical governing parameters is rather limited. These models have also been confirmed as an adequate tool for the study of steel connections; however their accuracy relies on the degree of refinement and accuracy of the assumed load–deformation laws for the principal components. The determination of such characteristics requires a complete understanding of the behaviour of single components, as well as of the way in which they interact, as a function of the geometrical and mechanical factors of the complete connections, [13].

Wales & Rossow [62] effectively introduced the use of mechanical models, or rather, a component-based method, when they developed a model for double web cleat connections, Fig. 1, in which the joint was idealised as two rigid bars connected by a homogeneous continuum of independent nonlinear springs. Each nonlinear spring was defined by a tri-linear load–deformation law obtained via the analysis of numerical models for the whole connection. Both bending moment and axial force were considered to act on the connection and coupling effects between the two stress resultants were then included in the joint stiffness matrix. Comparisons were made with a single test by Lewitt et al. [37] aiming to validate the philosophy. An important feature of this model is to account for the presence of the axial force. Results obtained by Wales & Rossow [62] indicate that greater attention should be given to such axial forces, as a factor affecting the response of beam-to-column connections.

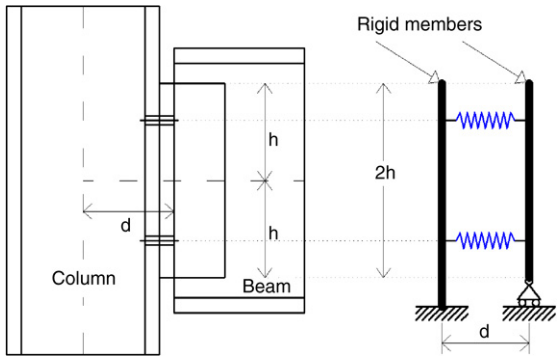

Fig. 1. Connection and mechanical model for web cleat connections, [62].

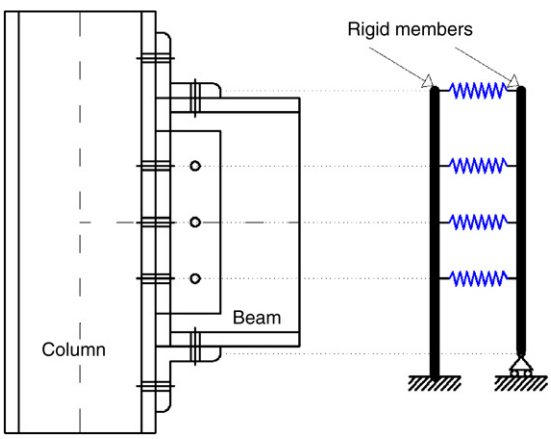

Fig. 2. Mechanical model for flange and web cleated connections, [64].

Kennedy & Hafez [63] used a technique of connection discretisation to describe the behaviour of header plate connections. T-stub models were used to represent the tension and compression parts of the connection. Although this model had provided good agreement with comparisons done against the author's own tests for ultimate moment capacity, the prediction of the corresponding rotations were not as accurate.

Chmielowiec & Richard [64] extended the model proposed by Wales & Rossow [62] to predict the behaviour of all types of cleated connections only subjected to bending and shear, Fig. 2. Mathematical expressions were adopted for the force–deformation relationships of the double angle segments and later calibrated by curve fitting against experimental results obtained by the same author. Comparisons with experimental data from a different series of connection tests in general confirmed the accuracy of the method.

An extensive investigation into the response of fully welded connections was conducted by Tschemmernegg [65], where the mechanical model of Fig. 3 was proposed. In this model, springs A are meant to account for the load introduction effect from the beam to the column, while springs B simulate the shear flexibility of the column web panel zone. Thirty tests were carried out, using a wide range of beam and column sections, making possible a calibration of the mathematical models assumed to describe the spring element properties. The moment–rotation curves for fully welded connections were determined via the model for all possible combinations of beams and columns made of European rolled sections IPE, HEA and HEB. This model was extended by Tschemmernegg & Humer [66] for endplate bolted connections by adding new springs (Fig. 4, springs C), to take into account the new sources of deformation. This model was also calibrated against experimental tests with good results.

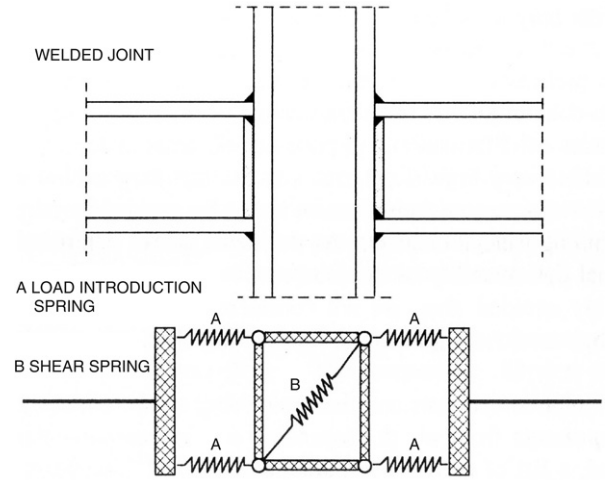

Fig. 3. Mechanical model for full welded joints, [65].

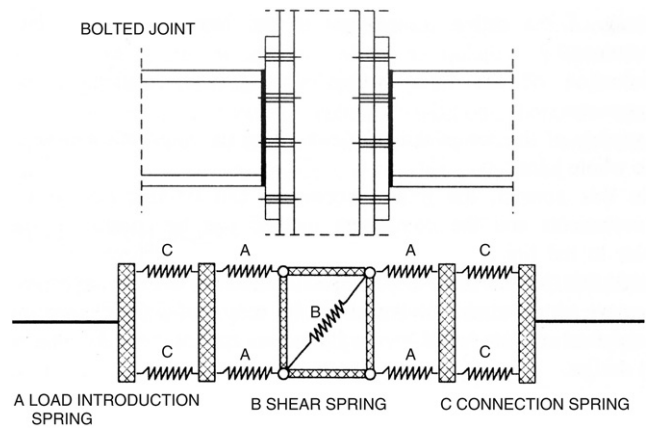

Fig. 4. Mechanical model for bolted joints, [66].

For 10 years, since the proposed model by Wales & Rossow [62] considering the bending moment and axial force interaction, nothing had been done in terms of these coupled effects until Madas [67] despite the fact that Wales & Rossow noted that greater attention should be given to such axial forces, as a factor affecting the response of beam-to-column connections. Madas [67] extended the mechanical model proposed by Wales & Rossow [62] to flexible endplate, double web angle and top and seat angle connections including both bare steel and composite connections. Fig. 5 shows the idealized beam-to-column connection used by Madas [67]. This model presented good agreement with experimental results; however it was not evaluated against experiments including the axial force versus bending moment interaction.

Based on preliminary studies carried out by Finet [68], Jaspart et al. [69] and Cerfontaine [70] developed a numerical approach aiming at analysing the joint behaviour from the first loading steps up to collapse, Fig. 6, subjected to bending moment and axial force. This approach is idealised by a mechanical model comprising extensional springs, Fig. 6(b). Each spring represents a joint component by exhibiting non-linear force–displacement behaviour, Fig. 6(c). Nunes [71] compared the experimental results obtained by Lima [72] for flush and extended endplate joints to the analytical results using the Cerfontaine [70] analytical model. This study pointed out some problems in the joint behaviour prediction using this analytical model, such as an overestimation of the initial stiffness in the majority of the cases, as well as variations between over and underestimation of the final moment capacity for some

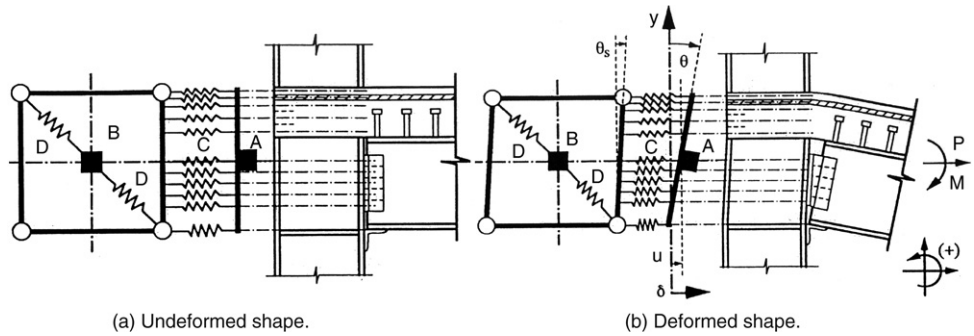

Fig. 5. Identification of beam-to-column connection, [67].

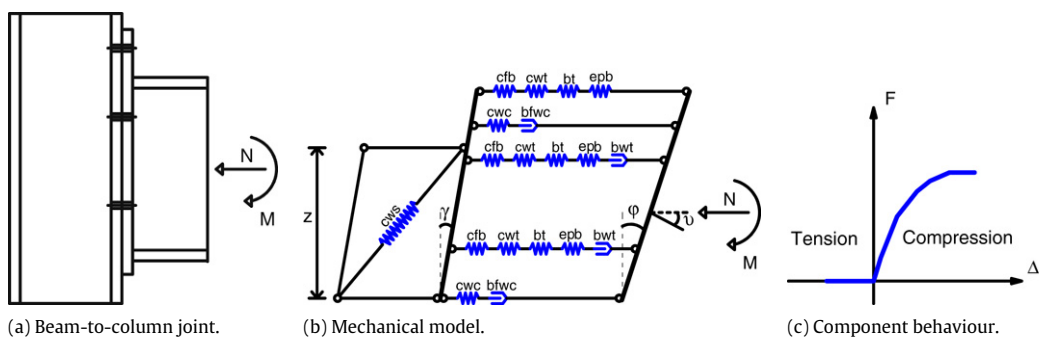

Fig. 6. Mechanical model, [69].

cases. These discrepancies were more pronounced for the cases in which the joints were subjected to bending moments and tensile axial forces.

A simplified mechanical model was suggested by Pucinotti [73] for top-and-seat and web angle connections as an extension of Eurocode 3 [74] to take into account the web cleats and hardening contributions. Comparisons against experimental tests showed that this model is able to estimate the initial stiffness accurately; however the final flexural capacity prediction is slightly erratic.

Using the same general principles, Simões da Silva & Coelho [75] formulated analytical expressions for the full non-linear response of a welded beam-to-column joint under combined bending moment and axial force. Each bi-linear spring of this model was replaced by two equivalent elastic springs using an energy formulation and a post-buckling stability analysis. A comparison was made against a welded joint only subjected to bending moments and the results presented a good agreement with the experiments.

Sokol et al. [76] developed an analytical model to predict the endplate joint behaviour subjected to bending moment and axial force interaction. This model was tested against two sets of experiments with flush endplate beam-to-beam joints and extended endplate beam-to-column joints carried out by Wald & Svarc [10]. In general, the results involving moment–rotation comparisons provided rather close agreement with the experimental tests, however, for all the analysed cases, the initial stiffness was overestimated whilst the final moment capacity was underestimated.

Lima [72] and Simões da Silva et al. [12] proposed mechanical models for extended (Fig. 7) and flush (Fig. 8) endplate joints, respectively. Following, basically, the same idea and also based on Madas [67], Ramli-Sulong [77] also developed a component-based connection model, Fig. 9, for flush and extended endplate, top-and-seat and/or web angles, and fin-plate connections. These models basically consist of two rigid bars representing the column centreline and the beam end, connected by non-linear springs that model the joint components. Furthermore, these authors included the compressive components (for instance, cwc—column web in compression, Figs. 7, 8 and 9) at the same location as the bolt rows and the tensile components (for example, cwt—column web in tension, Figs. 7 and 8) at the same location as the flanges (compressive rows). Proposed models by Lima [72] and Simões da Silva et al. [12] were tested against their own experimental tests. Although these models presented satisfactory results in terms of ultimate flexural capacity, the prediction of the initial stiffness, for the case of different axial load levels, was not accurate, predicting almost the same initial stiffness for the whole set of evaluated cases, Figs. 10 and 11. Regarding Ramli-Sulong's model [77,2], neither comparison has been done against experimental moment–rotation curves nor parametric analysis involving different axial force levels, which are needed to evaluate this model in terms of quality of moment–rotation curve prediction for moment-axial interaction. On the other hand, this model was shown to be able to predict, with a good accuracy, the experimental moment–rotation curves, disregarding the axial effect. Comparisons made at elevated temperature with available tests also presented a good agreement.

Urbonas & Daniunas [78] proposed a component method extension for endplate bolted beam-to-beam joints under bending and axial forces. However the procedure for joint moment–rotation curve prediction is only applicable and valid within the elastic regime of structural behaviour. Numerical tests were executed by the authors with a three-dimensional joint modelling using finite elements with the goal to validate this model. The results obtained for the beam-to-beam joint initial stiffness were close to the finite element analysis.

Table 1 presents a summary of the mechanical models for predicting joint behaviour discussed in this section.

Despite the continuous development and improvement of analytical models to predict the behaviour of joints under bending moment and axial force, there are still problems in the prediction of the moment–rotation curves, such as the joint initial stiffness for different axial force levels, as can be seen, for example, in Figs. 10 and 11 or in [71]. The magnitude of this problem increases when

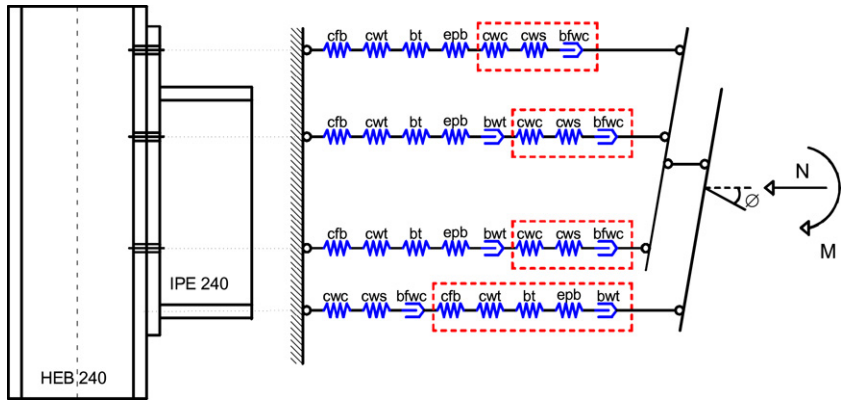

Fig. 7. Spring model for extended endplate joints, [72].

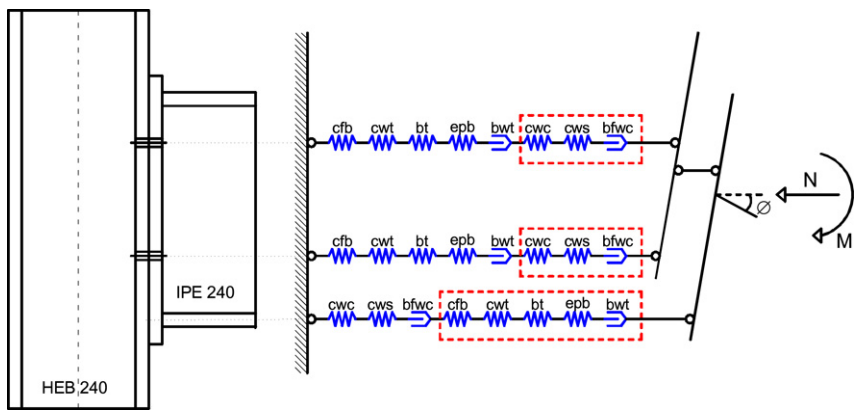

Fig. 8. Spring model for flush endplate joints, [72].

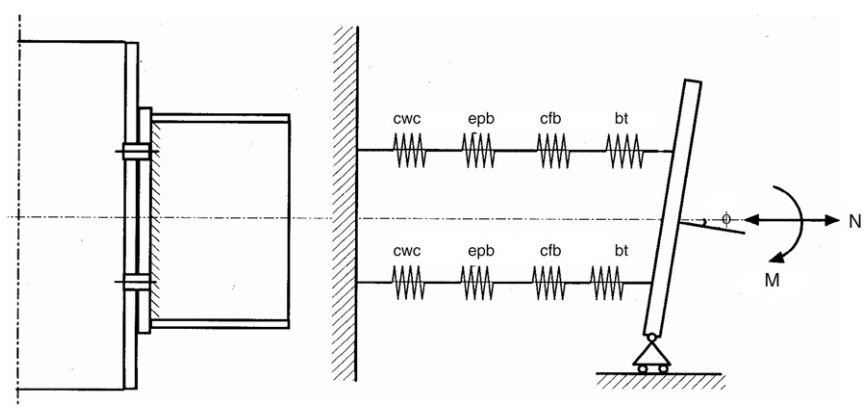

Fig. 9. Nonlinear spring connection model, [77].

joints are subjected to tensile axial forces. This problem relates to the ability of these models to deal with moment-axial interaction, and consequently changes of the compressive centre, before the first component yields. If the model is working on the linear-elastic regime, without reaching any component yield (i.e. the component stiffness is also working linearly), the modification of the joint stiffness matrix, only due to the geometric stiffness changes, will be insignificant. From this point upwards to the onset of first component yield, these models are not able to represent accurately the joint initial stiffness for any level of axial load and bending moment while working on the linear-elastic regime. Aiming to overcome this limitation, a mechanical model is proposed in this paper, which allows modifications of the compressive centre position even before reaching the first component yield, i.e. in the linear-elastic regime.

2. Generalised mechanical model for beam-to-column joints including the axial-moment interaction

The generalised model proposed for semi-rigid beam-to-column joints including the axial force versus bending moment interaction is depicted in Fig. 12. This model, based on the component method, contains three rigid bars representing the column centreline (support bar), the column flange centreline (second bar, b_2) and the beam end (first bar, b_1). These rigid bars are connected by a series of springs that model the joint components. The stiffness of these springs (rows) are representing by r_i, whilst u_i and ul_i are the absolute displacements of springs i referred to the first and second bars, respectively. C_i are the vertical coordinates of spring i.

Table 1
Summary of the mechanical models to predict the joint behaviour.

Authors (Reference)	Joint/Connection type	Forces
Wales & Rossow [62]	Double web cleat connections	Bending moment and axial force
Kennedy & Hafez [63]	Header plate connections	T-stub: axial force
Chmielowiec & Richard [64]	All types of cleated connections	Bending moment and shear
Tschemmernegg [65]	Welded connections	Bending moment
Tschemmernegg & Humer [66]	Endplate bolted connections	Bending moment
Madas [67]	Flexible endplate, double web angle and top and seat angle connections	Bending moment and axial force
Jaspart et al. [69] and Cerfontaine [70]	Extended and flush endplate connections	Bending moment and axial force
Pucinotti [73]	Top-and-seat and web angle connections	Bending moment
Simões da Silva & Coelho [75]	Welded beam-to-column joints	Bending moment and axial force
Sokol et al. [76]	Endplate joints	Bending moment and axial force
Lima [72]	Extended endplate joints	Bending moment and axial force
Lima [72] and Simões da Silva et al. [12]	Flush endplate joints	Bending moment and axial force
Ramli-Sulong [77]	Flush and extended endplate, top-and-seat and/or web angles, and fin-plate connections	Bending moment and axial force
Urbonas & Daniunas [78]	Endplate bolted beam-to-beam joints	Bending moment and axial force

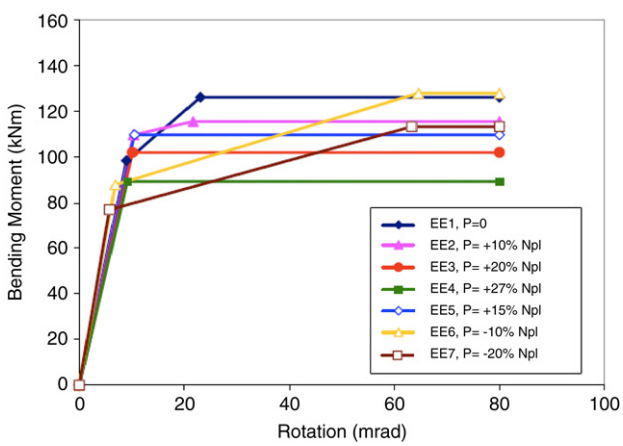

Fig. 10. Numerical simulations of the moment–rotation curves for the extended endplate joints, [72].

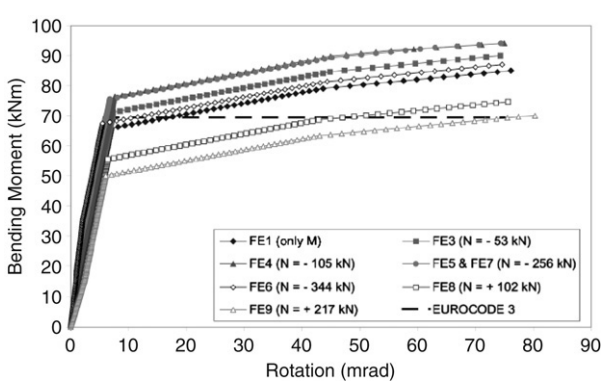

Fig. 11. Numerical simulations of the moment–rotation curves for the flush endplate joints, [12].

Due to the generalised formulation developed in this work, the model is able to represent any kind of connection, since the joint can be modelled according to the scheme shown in Fig. 12. The following sections present the adopted behaviour for each joint component as well as the complete formulation of this generalised mechanical model.

2.1. Characterisation of the joint components

The behaviour of each component of the joint is given by a force–deformation relationship, which may be characterised, for example, by a bi-linear, tri-linear or even a non-linear curve. Simões da Silva et al. [79], based on Kuhlmann et al. [80], classified the endplate joint components according to their ductility:

- Components with high ductility, Fig. 13(a): column web inshear (assuming no occurrence of local buckling), column flange in bending, endplate in bending and beam web in tension.
- Components with limited ductility, Fig. 13(b): column web in compression, column web in tension and beam flange in compression.
- Components with brittle failure, Fig. 13(c): bolts in tension and welds.

However, some comments are necessary regarding this classification:

- Eurocode 3 [4] considers a rigid-plastic behaviour for beam web in tension.
- Lima [72] verified a ductile behaviour for the beam flange in compression in his experiments.
- Welds are not considered in the joint rotation stiffness evaluation according to Eurocode 3 [4].

In this work, a tri-linear approach for the force–deformation relationship is suggested and used for all the joint components as shown in Fig. 14. The component elastic stiffness, k^e_{cp}, and the component yield strength, f^y_{cp}, are calculated according to the Eurocode 3 [4] component method. On the other hand, for the component plastic stiffness, a strain hardening stiffness k^p_{cp} is evaluated as:

$$k^p_{cp} = \mu^p k^e_{cp}. \tag{1}$$

The component reduced strain hardening stiffness, k^u_{cp}, referred to the component material fracture, is:

$$k^u_{cp} = \mu^u k^e_{cp} \tag{2}$$

where μ^p and μ^u are the strain hardening coefficients, respectively, for the plastic and ultimate stiffness, which depend on the component type. Based on the classification suggested by Simões da Silva et al. [79], briefly discussed in this paper, and curve fitting executed on the experimental tests carried out by Lima [72], Table 2 presents the values adopted for the strain hardening coefficient for each joint component.

The component ultimate capacity, f^u_{cp}, is determined, for each component, using the ultimate stress instead of the yield stress in equations present in [4].

For the case when the component related to the column web panel in shear is activated, i.e. when unbalanced moments exist in the connection, and the beam top flange and bottom flange of the connection are in compression, this component will be divided into two equal springs (one for the beam top flange and another for the beam bottom flange) characterised by its usual stiffness and yield and ultimate strengths divided by two.

The generalised mechanical model formulation, described in the next section, uses an effective stiffness for each model

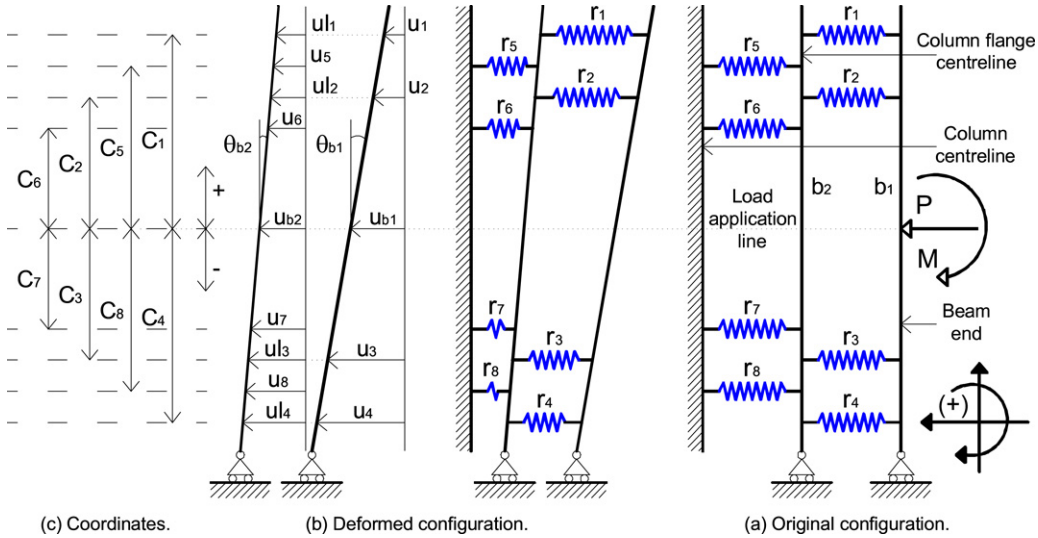

Fig. 12. Proposed generalised mechanical model for semi-rigid joints.

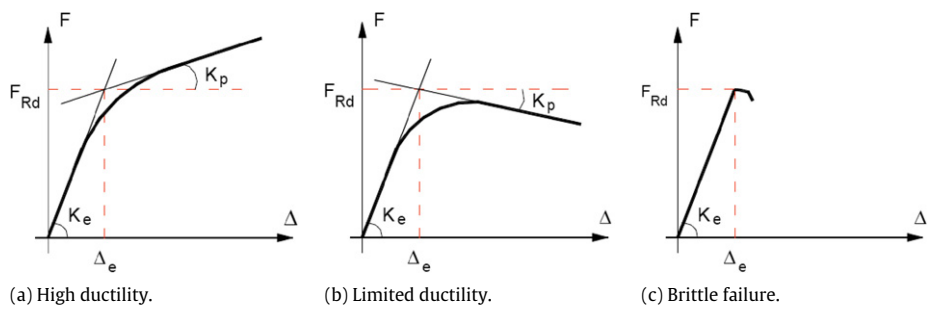

Fig. 13. Constitutive laws of the endplate joint components, [79].

row/spring i referred to the bolts and beam flanges, which is evaluated as:

$$r_i = \left\{ r_i^e = \frac{1}{\sum_{j=1}^{nc} \frac{1}{k_{cp}^e}} \text{ or } r_i^p = \frac{1}{\sum_{j=1}^{nc} \frac{1}{k_{cp}^p}} \text{ or } r_i^u = \frac{1}{\sum_{j=1}^{nc} \frac{1}{k_{cp}^u}} \right\} \tag{3}$$

where nc is the component number that contributes to the stiffness r_i of the row/spring i. The spring/row stiffness depends on the force–deformation relationship of each joint component that is evaluated according to the proposed procedure described in this section.

2.2. Generalised mechanical model formulation

The stationary potential energy principle was used to formulate the model stiffness matrix and the corresponding equilibrium equation. The total potential energy functional, Π, is:

$$\Pi = U - W \tag{4}$$

where U is the system strain energy and W is the load total potential. The system strain energy can be expressed in terms of the tangent stiffness r_i, Eq. (3), of the spring i, and relative displacements, Δ_i, as:

$$U = \frac{1}{2} \sum_{i=1}^{ns} r_i \Delta_i^2 \tag{5}$$

where ns is the system spring number. Assuming small displacements, the relative (Δ_i) and absolute (u_i and ul_i) displacements for the system presented in Fig. 12 can be evaluated as:

$$\begin{array}{ll} \text{Bar 1} & \text{Bar 2} \\ \Delta_i = u_i - ul_i & \Delta_i = u_i \\ u_i = u_{b1} - C_i \sin(\theta_{b1}) & u_i = u_{b2} - C_i \sin(\theta_{b2}) \\ ul_i = u_{b2} - C_i \sin(\theta_{b2}) & \end{array} \tag{6}$$

where C_i is the spring vertical coordinate i regarding the load application line. The spring coordinates above the loading application line must have a positive sign while the springs located below the loading application line should attain a negative sign. θ_{b1} and u_{b1}, θ_{b2} and u_{b2} are the rotations (θ_{bi}) and displacements (u_{bi}) of bars 1 and 2, respectively.

The system load total potential is, Fig. 12:

$$W = P(u_{b1} - u_{b2}) + M\theta_{b1} \tag{7}$$

where P is the axial load and M is the bending moment. Using the total potential energy principle, the equilibrium equations can be derived from the functional stationary condition Π (Eq. (4)),

$$\frac{\partial \Pi}{\partial d_i} = 0; \quad d_i = u_{b1}, \theta_{b1}, u_{b2}, \theta_{b2} \tag{8}$$

the stiffness matrix, K_{ij}, and internal load vector, F_i, can be derived using Eq. (5),

$$K_{ij} = \frac{\partial^2 U}{\partial d_i \partial d_j}; \quad d_i = u_{b1}, \theta_{b1}, u_{b2}, \theta_{b2} \tag{9}$$

$$F_i = \frac{\partial U}{\partial d_i}; \quad d_i = u_{b1}, \theta_{b1}, u_{b2}, \theta_{b2}. \tag{10}$$

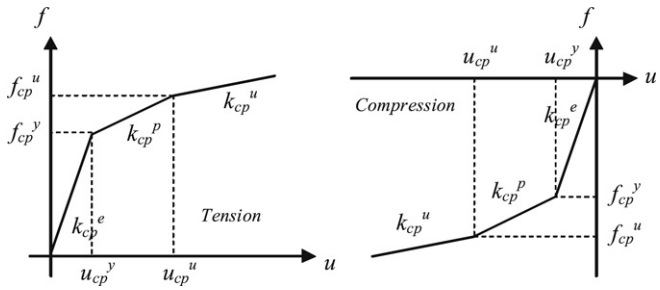

Fig. 14. Force–displacement curve for components in tension and compression.

Table 2
Values adopted for the strain hardening coefficients, μ.

Designation — Component	Plastic μ^p	Ultimate μ^u
1—Column web in shear	0.500	0.217
2—Column web in compression	0.300	0.130
3—Column web in tension	0.300	0.130
4—Column flange in bending	0.200	0.087
5—Endplate in bending	0.100	0.043
7—Beam or column flange and web in compression	∞	∞
8—Beam web in tension	∞	∞
10—Bolt in tension	0.600	0.261

Approximating the trigonometric expressions in Eq. (6) to the first order, the model stiffness matrix, Fig. 12, for any spring number at any position can be evaluated as:

$$\begin{bmatrix} K_{11}=\sum_{i=1}^{ns_{b1}} r_i & K_{12}=-\sum_{i=1}^{ns_{b1}} r_i C_i & K_{13}=-K_{11} & K_{14}=-K_{12} \\ & K_{22}=\sum_{i=1}^{ns_{b1}} r_i C_i^2 & K_{23}=-K_{12} & K_{24}=-K_{22} \\ & \textit{Symmetric} & K_{33}=\sum_{i=1}^{ns} r_i & K_{34}=-\sum_{i=1}^{ns} r_i C_i \\ & & & K_{44}=\sum_{i=1}^{ns} r_i C_i^2 \end{bmatrix} \quad (11)$$

where K_{11} and K_{33} are the matrix terms related to the axial deformations of the beam-to-column connection; K_{12} and K_{34} are associated with the interaction between the axial and the rotational deformations; K_{22} and K_{44} are correlated with the rotational deformations; ns and ns_{b1} is the number of springs of the model and between the first and second bars, respectively. The internal loading vector is:

$$F=\begin{bmatrix} P & M & 0.0 & 0.0 \end{bmatrix}^{\mathrm{T}}. \quad (12)$$

Due to the simplicity of this mechanical model formulation, it can be easily incorporated into a nonlinear semi-rigid joint finite element formulation, only requiring a tangent stiffness update procedure of each joint spring.

Regarding the first order approximations for the trigonometric expressions used in the generalised mechanical model formulation, Section 5 presents the error evaluation for these approximations versus joint rotations.

2.2.1. Analytical expressions: displacements and rotations

This section presents the analytical expressions for the displacements and the rotations of the proposed generalised mechanical model, Fig. 12. The main goal is to generate equations for the evaluation of these properties without executing a mechanical model numerical analysis.

Rewriting the equilibrium equations, Eq. (8), based on the symmetric stiffness matrix, Eq. (11), provides the complete equilibrium equations as a function of six stiffness terms, K_{11}, K_{12}, K_{22}, K_{33}, K_{34} and K_{44},

$$K_{11}u_{b1}+K_{12}\theta_{b1}-K_{11}u_{b2}-K_{12}\theta_{b2}=P \quad (13)$$

$$K_{12}u_{b1}+K_{22}\theta_{b1}-K_{12}u_{b2}-K_{22}\theta_{b2}=M \quad (14)$$

$$-K_{11}u_{b1}-K_{12}\theta_{b1}+K_{33}u_{b2}-K_{34}\theta_{b2}=0.0 \quad (15)$$

$$-K_{12}u_{b1}-K_{22}\theta_{b1}+K_{34}u_{b2}+K_{44}\theta_{b2}=0.0. \quad (16)$$

Isolating θ_{b2} from the equilibrium Eq. (16),

$$\theta_{b2}\left(u_{b1},\theta_{b1},u_{b2}\right)=\kappa u_{b1}+\lambda\theta_{b1}-\rho u_{b2} \quad (17)$$

where,

$$\kappa=\frac{K_{12}}{K_{44}};\qquad \lambda=\frac{K_{22}}{K_{44}};\qquad \rho=\frac{K_{34}}{K_{44}}. \quad (18)$$

Substituting θ_{b2}, Eq. (17), into the equilibrium equation (15), and isolating u_{b2},

$$u_{b2}\left(u_{b1},\theta_{b1}\right)=\frac{\omega_2 u_{b1}+\chi_2\theta_{b1}}{\psi} \quad (19)$$

where,

$$\psi=1-\frac{K_{34}^2}{K_{33}K_{44}};\qquad \omega_2=\frac{K_{11}}{K_{33}}-\frac{K_{34}K_{12}}{K_{33}K_{44}};\qquad \chi_2=\frac{K_{12}}{K_{33}}-\frac{K_{34}K_{22}}{K_{33}K_{44}}. \quad (20)$$

Substituting θ_{b2}, Eq. (17), into the equilibrium equation (14), and after substituting u_{b2}, Eq. (19), and subsequently isolating u_{b1},

$$u_{b1}\left(\theta_{b1},M\right)=\frac{M\psi-\theta_{b1}\mathrm{X}}{\Omega} \quad (21)$$

where,

$$\Omega=\omega_1\psi+\omega_2\xi;\qquad \mathrm{X}=\chi_1\psi+\chi_2\xi \quad (22)$$

$$\xi=\frac{K_{22}K_{34}}{K_{44}}-K_{12};\qquad \omega_1=\frac{K_{12}}{K_{44}}(K_{44}-K_{22});\qquad \chi_1=K_{22}-\frac{K_{22}^2}{K_{44}}. \quad (23)$$

Substituting θ_{b2} (Eq. (17)) into the equilibrium equation (13), u_{b2} (Eq. (19)), then u_{b1} (Eq. (21)), and subsequently isolating θ_{b1} generates the expression for the joint rotation (or first bar rotation), for any axial force and bending moment level:

$$\theta_{b1}\left(P,M\right)=\frac{P\Omega-M\vartheta\psi}{\mathrm{Z}} \quad (24)$$

where,

$$\mathrm{Z}=\varphi\Omega-\vartheta\mathrm{X} \quad (25)$$

$$\vartheta=K_{11}-\frac{K_{12}^2}{K_{44}}+\left(\frac{K_{11}K_{44}-K_{34}K_{12}}{K_{33}K_{44}-K_{34}^2}\right)\left(\frac{K_{12}K_{34}}{K_{44}}-K_{11}\right) \quad (26)$$

$$\varphi=K_{12}-\frac{K_{12}K_{22}}{K_{44}}+\left(\frac{K_{12}K_{44}-K_{34}K_{22}}{K_{33}K_{44}-K_{34}^2}\right)\left(\frac{K_{12}K_{34}}{K_{44}}-K_{11}\right). \quad (27)$$

Substituting θ_{b1} (Eq. (24)) into Eq. (21) leads to the joint horizontal displacement (first bar horizontal displacement):

$$u_{b1}\left(P,M\right)=\frac{P}{\vartheta}\left(1-\frac{\varphi\Omega}{\mathrm{Z}}\right)+\frac{M\varphi\psi}{\mathrm{Z}}. \quad (28)$$

Substituting θ_{b1} (Eq. (24)) and u_{b1} (Eq. (28)) into Eq. (19) produces the following expression for the second bar's horizontal displacement:

$$u_{b2}\left(P,M\right)=\frac{P}{\psi}\left[\frac{\omega_2}{\vartheta}\left(1-\frac{\varphi\Omega}{\mathrm{Z}}\right)+\frac{\chi_2\Omega}{\mathrm{Z}}\right]+\frac{M}{\mathrm{Z}}(\varphi\omega_2-\vartheta\chi_2). \quad (29)$$

Finally, substituting θ_{b1} (Eq. (24)), u_{b1} (Eq. (28)) and u_{b2} (Eq. (29)) into Eq. (17) leads to the expression for the second bar's rotation:

$$\theta_{b2}(P,M) = \frac{P}{Z}\left\{\frac{\kappa}{\vartheta}(Z-\varphi\Omega)+\lambda\Omega - \frac{\rho}{\psi}\left[\frac{\omega_2}{\vartheta}(Z-\varphi\Omega)+\chi_2\Omega\right]\right\} + \frac{M}{Z}[\kappa\varphi\psi-\lambda\vartheta\psi-\rho(\varphi\omega_2-\vartheta\chi_2)]. \quad (30)$$

With Eqs. (24) and (28)–(30) it is possible to evaluate all the joint displacements and rotations for any interaction level between axial force and bending moment, as well as, the forces in each spring:

$$f_i = r_i\Delta_i \quad (31)$$

where r_i and Δ_i are, respectively, the stiffness (Eq. (3)) and the relative displacement (Eq. (6)) of each spring.

2.2.2. Limit bending moments

For the correct use of the component method prior knowledge of which model rows (bolts and flanges) are in tension and/or compression is needed due to their effect on the evaluation of the joint rotation and flexural capacity. In the usual Eurocode 3 [4] mechanical model for joints subjected only to bending moment actions, a straightforward procedure is used to identify which rows are in compression and/or tension. However, when additional axial forces act on the joint, the identification whether each row is in tension or compression is not known in advance. This fact implies in the determination of the limit bending moment for the proposed mechanical model, Fig. 12, the need to identify when the row forces change from compression to tension or vice-versa. With these results in hand, it is possible to adopt a consistent component distribution to be used following the Eurocode 3 [4] principles. The limiting bending moment, for each j-spring (component) located between the first and second bars, can be obtained by isolating, u_{b1} from Eq. (6),

$$u_{b1} = \Delta_j + C_j\sin(\theta_{b1}) + u_{b2} - C_j\sin(\theta_{b2}) \quad (32)$$

substituting u_{b1} into the two first equilibrium equations, of Eq. (8),

$$\frac{\partial\Pi}{\partial u_{b1}} = 0 \quad (33)$$

$$\frac{\partial\Pi}{\partial\theta_{b1}} = 0. \quad (34)$$

This is followed by isolating θ_{b1} from the first equilibrium equation Eq. (33), then substituting it into the second equilibrium equation Eq. (34) and making the relative displacement (Δ_j) equal to zero, and finally isolating the bending moment to generate the following expression for the j-spring limit bending moment:

$$M_{j,\lim} = P\left(\frac{\sum_{i=1}^{ns_{b1}} r_iC_i^2 - C_j\left(\sum_{i=1}^{ns_{b1}} r_iC_i\right)}{C_j\left(\sum_{i=1}^{ns_{b1}} r_i\right) - \sum_{i=1}^{ns_{b1}} r_iC_i}\right) = P\left(\frac{K_{22}+C_jK_{12}}{C_jK_{11}+K_{12}}\right). \quad (35)$$

It is worth noting that Eq. (35) depends only on the axial load applied to the connection, and the stiffness and the vertical coordinates of springs located between the first and second bars. There is no significant influence of springs located between the second bar and supports on the limit bending moment evaluation.

According to Eq. (35), for instance, for the first spring ($j = 1$), for $M < M_{1,\lim}$ all rows are compressed; $M = M_{1,\lim}$ first spring axial force is equal to zero; and $M > M_{1,\lim}$ there are both tension and compression rows.

2.2.3. Moments that cause the joint rows and the joint to yield and reach failure

In this section analytical equations are derived, from the analytical expressions presented in Section 2.2, for the evaluation of bending moments that cause the model springs/rows and the joint to both yield and fail, for any axial force level.

The displacement Δ_i^y that causes the model spring/row i to yield is obtained by isolating Δ_i from Eq. (31), and setting f_i equal to the weakest component yield strength of spring/row i, f_{cp}^y,

$$\Delta_i^y = \frac{f_{cp}^y}{r_i^e}. \quad (36)$$

Similarly, the displacement Δ_i^u that causes the model spring/row i to fail is,

$$\Delta_i^u = \frac{f_{cp}^u}{r_i^p} \quad (37)$$

where r_i^e and r_i^p are the elastic and the plastic stiffness of the spring/row i, respectively, given in Eq. (3). The relative displacement of spring/row i located between the first and second bars, from Eq. (6), is,

$$\Delta_{br,i} = u_{b1} - C_i\sin(\theta_{b1}) - (u_{b2} - C_i\sin(\theta_{b2})). \quad (38)$$

Approximating the trigonometric expressions in Eq. (38) to the first order; then substituting u_{b1} (Eq. (28)), θ_{b1} (Eq. (24)), u_{b2} (Eq. (29)) and θ_{b2} (Eq. (30)) into it; and making the relative displacement ($\Delta_{br,i}$) equal to Δ_i^y (Eq. (36)) and subsequently isolating the bending moment generates the expression that causes the i-spring/row, located between the first and second bars, to yield:

$$M_{br,i}^y = \frac{\Delta_i^y + P(-\alpha_1+\alpha_2-C_i(\alpha_3-\alpha_4))}{\eta_1-\eta_2+C_i(\eta_3+\eta_4)}. \quad (39)$$

Similarly, making the relative displacement ($\Delta_{br,i}$) equal to Δ_i^u (Eq. (37)), the expression for the bending moment that causes the i-spring/row, located between the first and second bars, to fail is produced:

$$M_{br,i}^u = \frac{\Delta_i^u + P(-\alpha_1+\alpha_2-C_i(\alpha_3-\alpha_4))}{\eta_1-\eta_2+C_i(\eta_3+\eta_4)} \quad (40)$$

where the coefficients of Eqs. (39) and (40) are:

$$\begin{aligned}
\alpha_1 &= \frac{1}{\vartheta}\left(1-\frac{\varphi\Omega}{Z}\right)\\
\alpha_2 &= \frac{1}{\psi}\left[\frac{\omega_2}{\vartheta}\left(1-\frac{\varphi\Omega}{Z}\right)+\frac{\chi_2\Omega}{Z}\right]\\
\alpha_3 &= \frac{1}{Z}\left\{\frac{\kappa}{\vartheta}(Z-\varphi\Omega)+\lambda\Omega-\frac{\rho}{\psi}\left[\frac{\omega_2}{\vartheta}(Z-\varphi\Omega)+\chi_2\Omega\right]\right\}\\
\alpha_4 &= \frac{\Omega}{Z}\\
\eta_1 &= \frac{\varphi\psi}{Z}\\
\eta_2 &= \frac{\varphi\omega_2-\vartheta\chi_2}{Z}\\
\eta_3 &= \frac{\kappa\varphi\psi-\lambda\vartheta\psi-\rho(\varphi\omega_2-\vartheta\chi_2)}{Z}\\
\eta_4 &= \frac{\vartheta\psi}{Z}.
\end{aligned} \quad (41)$$

Following the same idea, now, for spring/row i located between the second bar and supports, the relative displacement, from Eq. (6), is,

$$\Delta_{fr,i} = u_{b2} - C_i\sin(\theta_{b2}). \quad (42)$$

Approximating the trigonometric expressions in Eq. (42) to the first order; then substituting u_{b2} (Eq. (29)) and θ_{b2} (Eq. (30)) into it; and making the relative displacement ($\Delta_{fr,i}$) equal to Δ_i^y

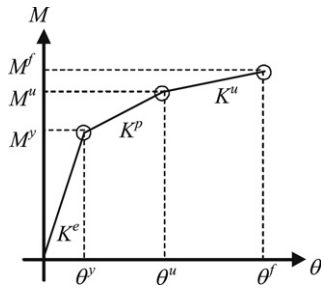

Fig. 15. Proposed prediction of the bending moment versus rotation curve for any axial force level.

(Eq. (36)) and subsequently isolating the bending moment produces the expression that causes the i-spring/row, located between the second bar and supports, to yield:

$$M^y_{fr,i} = \frac{\Delta^y_i + P\left(-\alpha_2 + C_i\alpha_3\right)}{\eta_2 - C_i\eta_3}. \tag{43}$$

Similarly, making the relative displacement ($\Delta_{fr,i}$) equal to Δ^u_i (Eq. (37)) leads to the following expression for the bending moment that causes the i-spring/row, located between the second bar and supports, to fail:

$$M^u_{fr,i} = \frac{\Delta^u_i + P\left(-\alpha_2 + C_i\alpha_3\right)}{\eta_2 - C_i\eta_3} \tag{44}$$

where the coefficients of Eqs. (43) and (44) are given in Eq. (41).

Finally, the joint yield bending moment can be calculated as being the minimum yield bending moment given in Eqs. (39) and (43),

$$M^y = \min\{M^y_{br,i} \rightarrow \text{Eq. (39)}, M^y_{fr,i} \rightarrow \text{Eq. (43)}\} \tag{45}$$

and the joint plastic bending moment as being the minimum plastic bending moment evaluated by Eqs. (40) and (44),

$$M^u = \min\{M^u_{br,i} \rightarrow \text{Eq. (40)}, M^u_{fr,i} \rightarrow \text{Eq. (44)}\}. \tag{46}$$

The joint rotational capacities, θ^y and θ^u, referred to the joint yield and plastic bending moments are, respectively,

$$\theta^y = \frac{P\Omega - M^y\vartheta\psi}{Z} \tag{47}$$

$$\theta^u = \frac{P\Omega - M^u\vartheta\psi}{Z}. \tag{48}$$

For a given joint rotation (θ) and axial force (N), it is also possible to calculate the corresponding joint bending moment by isolating it from Eq. (24),

$$M = \frac{P\Omega - \theta Z}{\vartheta\psi}. \tag{49}$$

The analytical expressions developed in this section provide all the necessary information to predict bending moment versus rotation curves for any axial force level applied to the joint.

2.3. Prediction of bending moment versus rotation curve for any axial force level

Based on the equations previously developed, Fig. 15 presents an approach to characterise bending moment versus rotation curves considering the bending moment versus axial force interaction.

For each moment–rotation curve, the first point (θ^y, M^y) defines the joint initial stiffness corresponding to the attainment of the weakest component yield while the second point (θ^u, M^u) is obtained when the weakest component reaches its ultimate strength. The third point (θ^f, M^f) depends on the joint assumed final rotational capacity for the moment–rotation curve. In this work a 0.05-rad joint final rotation was adopted based on studies for both frames and individual restrained member. The joint rotations required at maximum load have shown that behaviour at rotations beyond 0.05 rad, often much less, has little practical significance, [13].

Summarising, the points of the moment–rotation curve are:

$$\begin{array}{lll} Pnt\ 1 & \theta^y \rightarrow \text{Eq. (47)}; & M^y \rightarrow \text{Eq. (45)} \\ Pnt\ 2 & \theta^u \rightarrow \text{Eq. (48)}; & M^u \rightarrow \text{Eq. (46)} \\ Pnt\ 3 & \theta^f = 0.05\ \text{rad}; & M^f \rightarrow \text{Eq. (49)}. \end{array} \tag{50}$$

It is worth highlighting that more points could have been used to describe the bending moment versus rotation curve because, for instance, before reaching the joint plastic bending moment other joint rows might start yielding by generating new points between the first and second points (Eq. (50)) changing the joint stiffness matrix. However, for simplicity of the approach and examples described in Section 3, three points were adopted.

2.4. Lever arm d

The lever arm d represents the tensile rigid link position that unites the second bar to the supports, as can be seen, for instance, in Fig. 16. On Fig. 16, k_{br1}, k_{br2}, k_{br3} represent the elastic stiffness of bolt-rows 1, 2 and 3, respectively; k_{bbf} is the elastic stiffness of the bottom flange of the beam; k_{lcbf} is the compressive rigid link associated with the bottom flange of the beam; and k_{lt} is the elastic stiffness of the tensile rigid link referred to the lever arm.

The evaluation of this lever arm d is needed when a mechanical model is adopted as in Fig. 16, where the first bolt rows are in tension, i.e., the beam top flange is not under compression. According to Del Savio et al. [81], the joint initial stiffness is strongly influenced by this lever arm d. Based on this fact, an approach is here presented for evaluation of this lever arm d which is divided into two equations: one for compressive forces (Section 2.4.2) and another for the complementary cases disregarding axial forces and/or considering tensile forces (Section 2.4.1) applied to the joint.

2.4.1. Lever arm evaluation for the complementary cases disregarding axial forces and/or considering tensile forces applied to the joint

Considering the support reactions and the applied loads, Fig. 16, the system force equilibrium can be evaluated as:

$$F_{bbf} - F_{linkt} = P. \tag{51}$$

The system moment equilibrium at the beam bottom flange is:

$$F_{linkt}\left(d + e\right) + Pe = M \tag{52}$$

where F_{bbf} is the row compressive yield capacity referred to the beam bottom flange; F_{linkt} is the rigid link tensile capacity that joins the second bar to the supports; d and e are, respectively, the distances from the loading application centre to the rigid link and the beam bottom flange.

Assuming M to be equal to the yield bending moment of the first bolt-row $M^y_{br,1}$ given in Eq. (39), F_{bbf}, P and e are already known, the problem variables are F_{linkt} and d. Then, isolating F_{linkt} from Eq. (51), substituting it into Eq. (52), and then isolating d leads to the expression for the lever arm position:

$$d = \frac{Pe - M^y_{br,1}}{P - F_{bbf}} - e \tag{53}$$

which also satisfies the condition where F_{bbf} and $M^y_{br,1}$ simultaneously reach the yield.

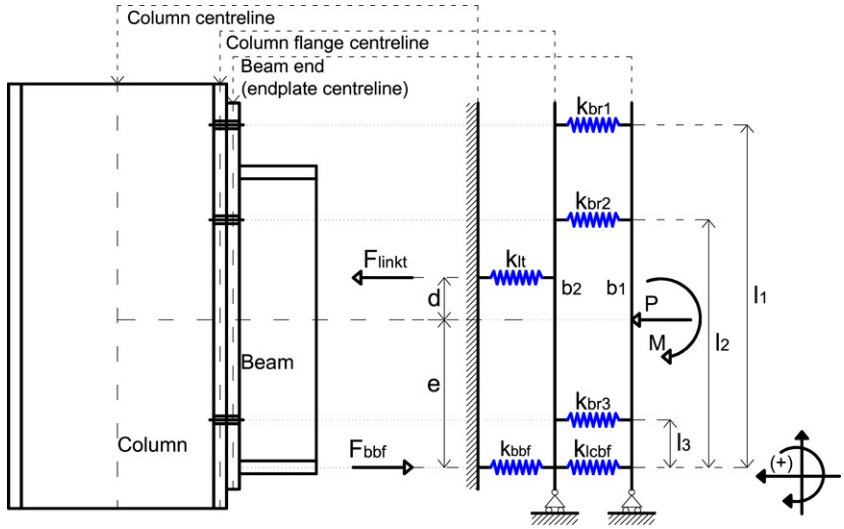

Fig. 16. Proposed generalised mechanical model for semi-rigid joints – lever arm *d*.

2.4.2. Lever arm evaluation for compressive forces applied to the joint

The lever arm *d* for these cases is evaluated as the ratio between the sum of bending moments referred to the bolt-rows and the axial force at the beam bottom flange and the sum of forces referred also to the bolt-rows and the axial force minus the distance from the load application centre to the beam bottom flange:

$$d = \frac{\sum_{i=1}^{nbr} f_{br,i}^{y} l_i + Pe}{\sum_{i=1}^{nbr} f_{br,i}^{y} + P} - e \tag{54}$$

where *nbr* is the number of joint bolt-rows, $f_{br,i}^{y}$ is the yield strength of bolt-row *i* and l_i is the distance from joint bolt-row *i* to the beam bottom flange centre.

The lever arm *d* evaluated in either Eq. (53) or Eq. (54) take into account the change of the joint compressive centre position according to the axial force levels and bending moment applied to the joint, before the yield of the first weakest component is reached.

3. Application of the proposed generalised mechanical model

Application of the generalised mechanical model, developed in Section 2, to predict the joint behaviour requires the following steps:

(a) Generation and adoption of a joint model in consonance with the generalised mechanical model presented in Fig. 12.
(b) Joint design according to Eurocode 3 [4].
(c) Characterisation of the joint components: force–displacement relationship of each component according to the approach suggested in Section 2.1.
(d) Identification of all the possible situations (model for compression, tension, tension/compression) given that loading may vary from pure bending to pure compressive/tensile axial force with all intermediate combinations. These intermediate combinations are derived from the adopted model in step (a).
(e) Evaluation of the limit bending moments for the adopted models in step (d), with the aid of Eq. (35), to define the application domains of each one.
(f) Evaluation of the lever arm *d* according to the proposed procedure in Section 2.4, Eq. (54) for compressive forces and Eq. (53) for either tensile forces or without axial forces, considering the change of the joint compressive centre position.
(g) Prediction of bending moment versus rotation curves for each axial force level, according to the approach described in Section 2.3.

It is worth highlighting that the incorporation of this approach into a nonlinear semi-rigid joint finite element formulation does not require steps (d) and (e), because the complete joint modelling already considers all the possible situations of loading through each component force–displacement characteristic curve. In order to explain how each step is evaluated, six extended endplate joints tested by Lima et al. [11] were modelled.

3.1. Extended endplate joints

Starting with the application of step (a) previously described and using the extended endplate joint properties, Fig. 17, the following mechanical model was adopted, Fig. 18. In Fig. 18, k_{br1}, k_{br2}, k_{br3} represent the elastic stiffness of bolt-rows 1, 2 and 3, respectively. k_{lt1}, k_{lt2}, k_{lt3} are the elastic stiffness of the tensile rigid links referred to the bolt-rows 1, 2 and 3, respectively. k_{btf} and k_{bbf} are the elastic stiffness of the top and bottom flanges of the beam. k_{lctf} and k_{lcbf} are the compressive rigid links associated with the top and bottom flanges of the beam. k_{lt} is the elastic stiffness of the tensile rigid link referred to the lever arm.

Next step (b), with the joint material (Table 3) and geometric (Fig. 17) properties, the theoretical values of the strength and initial stiffness for the extended endplate joint components are evaluated according to Eurocode 3 [4] and are presented in Table 4.

With the evaluated properties of the joint components, the characterisation of the force–displacement relationship for each component can be calculated according to the proposed formulation. Table 5 presents the results of this step (c).

Based on the adopted mechanical model, step (a), Fig. 18, four derived models are identified and presented in Fig. 19. These four models, referred to step (d), are able to deal with the eight load situations presented in Table 6. For the experimental tests used in this section, only three load situations depicted in Table 6 were necessary:

- Number 3, where only bending moment is applied to the joint and the proposed model presented in Fig. 19(c) is sufficient to model the joint.

- Number 5, where a compressive axial force is applied to the joint followed by a bending moment increase. This situation uses the proposed models depicted in Fig. 19(a) and (c).

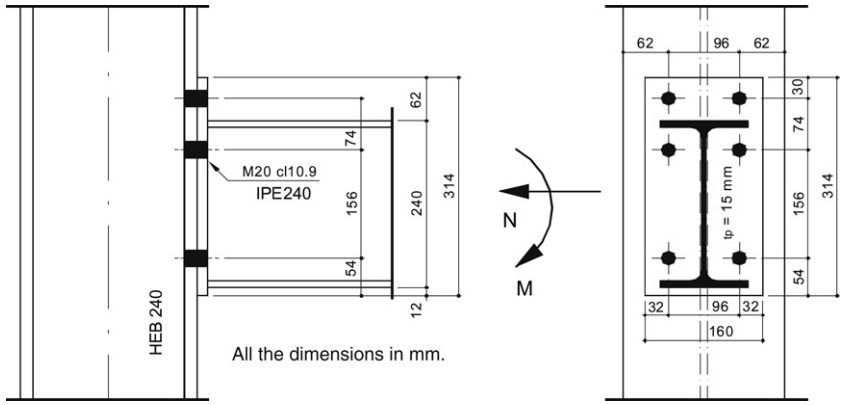

Fig. 17. Extended endplate joint, [11].

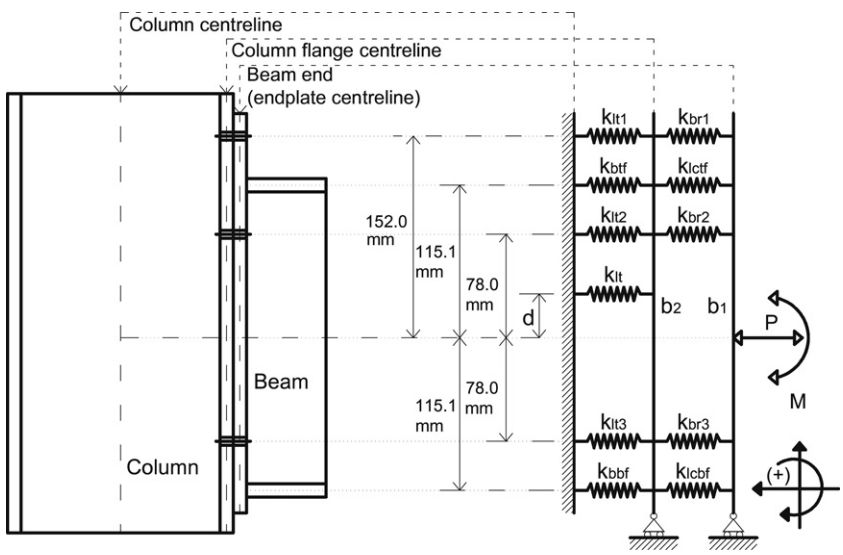

Fig. 18. Proposed mechanical model.

Table 3
Steel mechanical properties.

Specimen		Yield strength (MPa)	Ultimate strength (MPa)	Young's modulus (MPa)	Ratio yield/Ultimate
Beam	Web	363.40	454.30	203,713	1.250
IPE 240	Flange	340.14	448.23	215,222	1.318
Column	Web	372.02	477.29	206,936	1.283
HEB 240	Flange	342.95	448.79	220,792	1.309
Endplate		369.44	503.45	200,248	1.363
Bolts		900.00	1000.00	210,000	1.111
Weld		–	576.00	210,000	–

- Number 6, where a tensile axial force is first applied to the joint with a subsequent bending moment application. In this case, the proposed models in Fig. 19(b) and (c) are utilised.

Before analysing the adopted mechanical models in Fig. 19, it is necessary to identify each model applicability domain, which depends on whether the joint components are subjected to either compression or tension, for a given combination of bending moment and axial force. This is done by evaluating the limit bending moments (M_{lim}), step (e), for the adopted models in Fig. 19 with the aid of Eq. (35), relative to the experimental axial force levels. This step does not require a knowledge of the lever arm position d since the yield of joint bolt-rows is not affected by this position. In this case, only the joint rotation and the joint row yield corresponding to the beam flanges are affected. The results of the limit bending moment evaluations are illustrated in Table 7. For the EE1 experiment (load situation number 3, Table 6) any bending moment applied to the joint model, Fig. 19(c), induces tension on the joint first bolt row and compression on the beam bottom flange. For the EE2, EE3 and EE4 experimental tests (load situation number 5, Table 6), the limit bending moment, which induces tension on the beam top flange is obtained by using the proposed mechanical model shown in Fig. 19(a). For the EE6 and EE7 tests (load situation number 6, Table 6), the limit bending moment, which leads the third bolt row to compression, is calculated by the proposed mechanical model illustrated in Fig. 19(b).

Based on these limit bending moments, an appropriate mechanical model can then be adopted from those shown in Fig. 19. For instance, for EE4 test if the bending moment applied to the joint were smaller than 34.55 kN m, Table 7, the compressive model presented in Fig. 19(a) should be used. For larger values the tensile–compressive model should be utilised. On the other hand, if the proposed mechanical model, Fig. 18, were implemented into a nonlinear structural analysis program, where each component was described by its force–displacement characteristic curve,

Table 4
Theoretical values of the resistance and initial stiffness of the extended endplate joint components, Fig. 17, evaluated according to Eurocode 3 [4].

Component		f_{cp}^{y} (kN)	k_{cp}^{e} (kN/mm)	f_{i}^{y} (kN)	r_{i}^{e} (kN/mm)
Beam top and bottom flange (compression)	cwc	656.7	2133.6	**321.3**	**464.8**
	bfc	541.6	∞		k_{btb} /k_{bbf}
	cws	**321.3**	594.3		
Beam bottom flange	cwc	656.7	2133.6	**541.6**	**763.4**
	bfwc	**541.6**	∞		k_{bbf}
	cws	642.5	1188.6		
First bolt row ($h = 267.1$ mm)	cwt	533.2	1476.3	**289.8**	**607.7**
	cfb	311.3	8499.7		k_{br1}
	epb	**289.8**	4223.1		
	bt	441.0	1630.6		
Second bolt row ($h = 193.1$ mm)	Considered individually				
	cwt	445.4	1476.3	**218.6**	**575.0**
	cfb	218.6	8498.7		k_{br2}
	epb	326.9	3026.1		
	bwt	492.3	∞		
	bt	441.0	1629.6		
	cwc	366.9			
	bfwc	251.6			
	cws	352.8			
	Bolt-row belonging to the bolt group: bolt-rows 2 + 1				
	cwt	735.1			
	cfb	508.4			
	epb	616.7			
Third bolt row ($h = 37.1$ mm)	Considered individually				
	cwt	410.3	1476.3	**33.3**	**554.7**
	cfb	311.3	8498.7		k_{br3}
	epb	320.3	2538.9		
	bwt	413.2	∞		
	bt	441.0	1629.6		
	cwc	148.3			
	bfwc	**33.3**			
	cws	134.2			
	Bolt row belonging to the bolt group: bolt rows 3 + 2				
	cwt	350.8			
	cfb	663.4			
	epb	623.9			
	bwt	764.7			
	Bolt row belonging to the bolt group: bolt rows 3 + 2 + 1				
	cwt	918.7			
	cfb	878.8			
	cws	898.2			

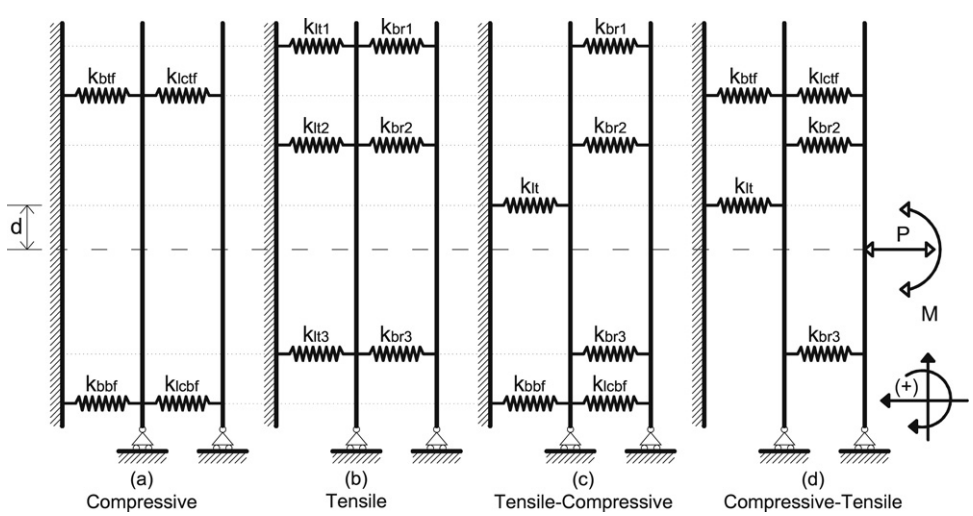

Fig. 19. Proposed mechanical model for each analysis stage.

Table 5
Characterisation of the extended endplate joint components, Fig. 17, according to the approach given in Section 2.1.

Component		f_{cp}^u (kN)	k_{cp}^p (kN/mm)	k_{cp}^u (kN/mm)	f_i^u (kN)	r_i^p (kN/mm)	r_i^u (kN/mm)
Beam top and bottom flange (compression)	cwc	842.6	640.1	278.3	**412.2**	**202.9**	**88.2**
	bfc	695.4	∞	∞			k_{btb} /k_{bbf}
	cws	**412.2**	297.2	129.2			
Beam bottom flange	cwc	842.6	640.1	278.3	**695.4**	**308.3**	**134.0**
	bfc	**695.4**	∞	∞			k_{bbf}
	cws	824.4	594.3	258.4			
First bolt row ($h = 267.1$ mm)	cwt	684.2	442.9	192.6	**394.9**	**160.3**	**69.7**
	cfb	407.5	1699.7	739.04			k_{br1}
	epb	**394.9**	422.3	183.6			
	bt	490.0	977.8	425.1			
Second bolt row ($h = 193.1$ mm)	Considered individually						
	cwt	571.4	442.9	192.6	**286.1**	**139.4**	**60.6**
	cfb	**286.1**	1699.7	739.0			k_{br2}
	epb	445.5	302.6	131.6			
	bwt	615.4	∞	∞			
	bt	490.0	977.8	425.1			
	cwc	466.8					
	bfwc	320.1					
	cws	448.8					
	Bolt row belonging to the bolt group formed by bolt rows 2 + 1						
	cwt	943.2					
	cfb	665.3					
	epb	840.3					
Third bolt row ($h = 37.1$ mm)	Considered individually						
	cwt	526.5	442.9	192.6	**42.3**	**128.1**	**55.7**
	cfb	407.5	1699.7	739.0			k_{br3}
	epb	436.5	253.9	110.4			
	bwt	516.6	∞	∞			
	bt	490.0	977.8	425.1			
	cwc	188.7					
	bfwc	**42.3**					
	cws	170.7					
	Bolt row belonging to the bolt group formed by bolt rows 3 + 2						
	cwt	1178.7					
	cfb	1150.2					
	epb	1223.9					
	bwt	956.0					
	Bolt row belonging to the bolt group formed by bolt rows 3 + 2 + 1						
	cwt	1178.7					
	cfb	1150.2					
	epb	1223.9					

f_{cp}^u is given in Section 2.1, k_{cp}^p and k_{cp}^u are given in Eqs. (1) and (2), respectively.

these joint components would be automatically activated or deactivated according to its compressive/tensile characteristic (Fig. 14), without the need to previously define a model for each load situation as shown in Fig. 19 and Table 6.

The proposed mechanical models presented in Fig. 19(c) and (d) require the evaluation of the lever arm d, step (f). Table 7 presents the lever arm d positions evaluated for the mechanical model shown in Fig. 19(c), where Eq. (54) is used for compressive forces applied to the joint and Eq. (53) is utilised for all the other complimentary cases. Regarding the mechanical model in Fig. 19(d), the lever arm d positions were not calculated since they were not considered in the Lima et al. [11] experiments.

Finally, with the steps (a) to (f) evaluated for the adopted model in Fig. 19, it is possible to predict the bending moment versus rotation curves for each axial force level, step (g), used in the experimental tests carried out by Lima et al. [11]. Table 8 presents the values evaluated for each moment–rotation curve, according to the approach described in Section 2.3. Point 1 (θ^y, M^y), Table 8, defines the onset of the joint yield and is evaluated in Eq. (50), by using the yield strength (Table 4, f_i^y) and the elastic effective stiffness (Table 4, r_i^e) for rows i. Point 2 (θ^u, M^u) represents the joint ultimate capacity and is obtained by utilising Eq. (50) and the ultimate strength (Table 5, f_i^u) and the plastic effective stiffness (Table 5, r_i^p) for rows i. Point 3 (θ^f, M^f), Eq. (50), is obtained by adopting a 0.05-rad final rotation for the joint and the reduced strain hardening effective stiffness (Table 5, r_i^u) for rows i. With these results in hand, the results of each analysis compared to their equivalent experimental tests are illustrated in Fig. 20(a) to (f). Subsequently, Fig. 21 presents the whole set of numerical results.

4. Results and discussion

Six experimental moment–rotation curves, of Lima et al. [11], were used to validate the proposed mechanical model in Section 2 as well as to demonstrate its application.

Fig. 20(a) illustrates the comparisons between the proposed model and the EE1 test moment–rotation curve that was only subjected to bending moments. For this case, the point that characterises the joint initial stiffness was defined at 2/3 of M_{jrd} (joint design bending moment) according to Eurocode 3 [4]—tri-linear approach, being the point M_{jrd} defined by yielding of the

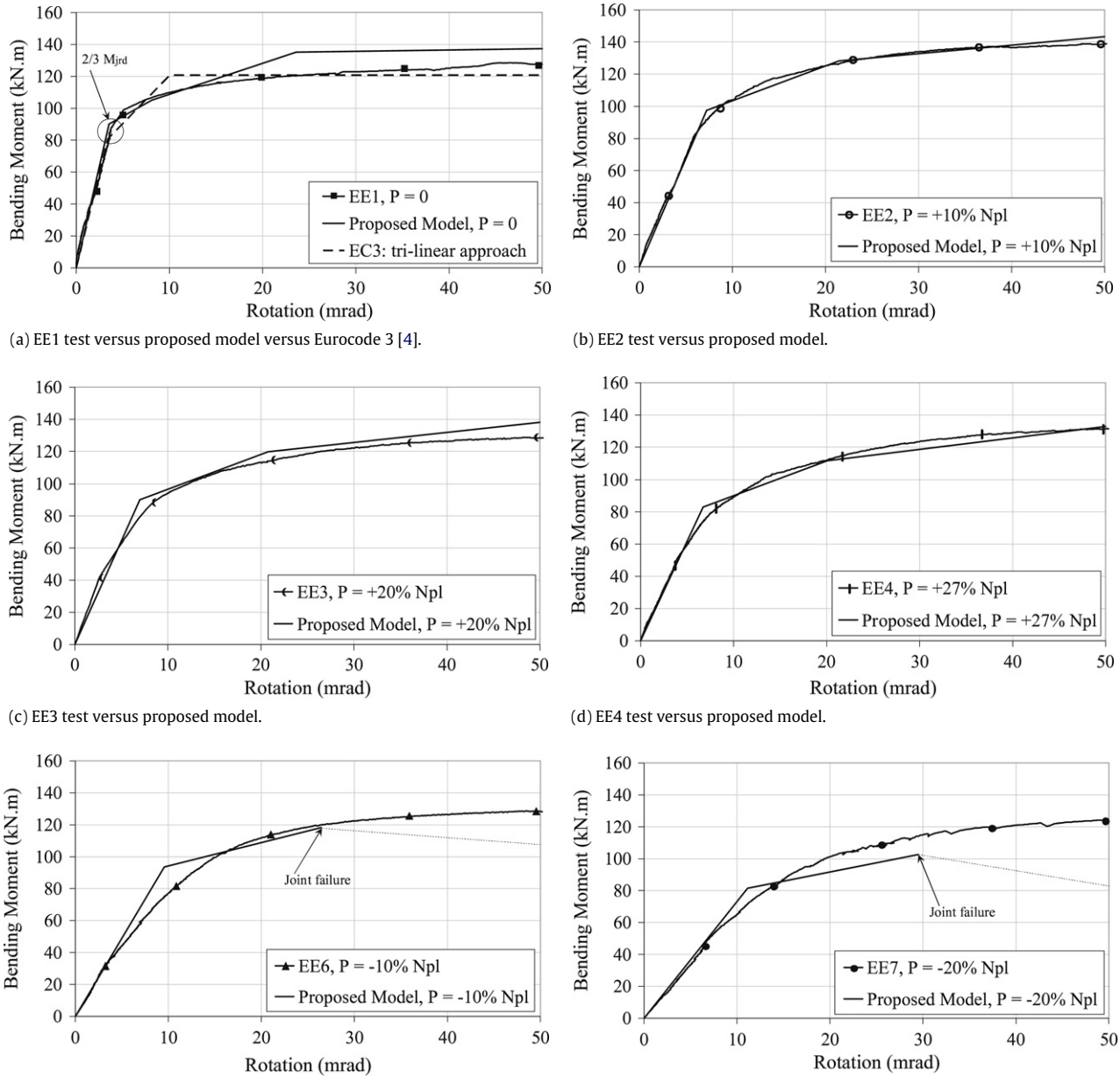

(a) EE1 test versus proposed model versus Eurocode 3 [4].

(b) EE2 test versus proposed model.

(c) EE3 test versus proposed model.

(d) EE4 test versus proposed model.

(e) EE6 test versus proposed model.

(f) EE7 test versus proposed model.

Fig. 20. Comparisons between experimental moment–rotation curves, by Lima et al. [11], and predicted curves by using the proposed mechanical model.

Table 6
Load situations applied to the joint and their respective mechanical models.

N^o	Load situations		Mechanical model (s)
	Bending moment	Axial force	
1	–	$+P$	Compressive, Fig. 19(a)
2	–	$-P$	Tensile, Fig. 19(b)
3	$+M$	–	Tensile–compressive, Fig. 19(c)
4	$-M$	–	Compressive–tensile, Fig. 19(d)
5	$+M$	$+P$	Fig. 19(a) and (c)
6	$+M$	$-P$	Fig. 19(b) and (c)
7	$-M$	$+P$	Fig. 19(a) and (d)
8	$-M$	$-P$	Fig. 19(b) and (d)

$+P$ and $-P$ are compressive and tensile axial forces applied to the joint, respectively. $+M$ is the bending moment that compresses the beam bottom flange and tensions the beam top flange, whilst $-M$ is the bending moment that tensions the beam bottom flange and compresses the beam top flange.

endplate in bending. The initial stiffness is slightly overestimated by 10% by the mechanical model whilst the flexural capacity is rather over-predicted by 14%, Table 9. In comparison with Eurocode 3 [4] the proposed mechanical model overestimates the initial stiffness and the flexural capacity by 7% and 12%, respectively. The discrepancies between the Eurocode 3 [4] and the proposed mechanical model results are due to a different assumption for the joint rotation centre, which for Eurocode 3 [4] is assumed at the beam bottom flange while for the proposed approach it is given by lever arm d evaluated according to the proposed procedure in Section 2.4.

Fig. 20(b), (c) and (d) present comparisons between the proposed model and moment–rotation curves of EE2, EE3 and EE4 tests that respectively consider compressive forces of 10%, 20% and 27% of the beam axial plastic capacity. For these three compressive cases, the joint initial stiffness was defined by yielding of the beam bottom flange in compression. Very good correlation between the experimental tests and numerical results was obtained, Table 9.

Fig. 20(e) and (f) illustrate the results for EE6 and EE7 moment–rotation curves that respectively consider tensile forces

Table 7
Applicability of each model, M_{lim}, and evaluation of lever arm d according to the experimental axial force levels.

Experimental data		M_{lim} (kN m), Eq. (35)			Lever arm (mm)
Test	N (kN)	Compressive Fig. 19(a)	Tensile Fig. 19(b)	Tensile-compressive Fig. 19(c)	
EE1 (only M)	0.00	NA[a]	NA[a]	0.00 to M^f	Eq. (53): 79.28
EE2 (+10% N_{pl})	135.94	0.0 to 18.12	NA[a]	18.12 to M^f	Eq. (54): 86.34
EE3 (+20% N_{pl})	193.30	0.0 to 25.77	NA[a]	25.77 to M^f	Eq. (54): 79.60
EE4 (+27% N_{pl})	259.20	0.0 to 34.55	NA[a]	34.55 to M^f	Eq. (54): 73.05
EE6 (−10% N_{pl})	−127.20	NA[a]	0.0 to 15.96	13.73 to M^f	Eq. (53): 46.57
EE7 (−20% Npl)	−257.90	NA[a]	0.0 to 32.36	27.84 to M^f	Eq. (53): 24.33

"+" indicates compressive axial forces and "−" tensile axial forces. M^f is given in Eq. (50).
[a] NA = not applicable.

Table 8
Values evaluated for the prediction of the moment–rotation curves for different axial force levels.

Point	EE1 (only M)		EE2 (+10% N_{pl})		EE3 (+20% N_{pl})		EE4 (+27% N_{pl})		EE6 (−10% N_{pl})		EE7 (−20% N_{pl})	
	θ (mrad)	M (kN m)	θ (mrad)	M (kN m)	θ (mrad)	M (kN m)	θ (mrad)	M (kN m)	θ (mrad)	M (kN m)	θ (mrad)	M (kN m)
	0.0	0.0	0.0	0.0	0.0	0.0	0.0	0.0	0.0	0.0	0.0	0.0
1	8.2	105.3	7.2	97.4	7.0	90.1	6.7	83.0	9.6	93.5	11.1	81.4
2	23.6	135.1	21.4	128.2	20.8	119.9	20.1	111.8	26.4	118.3	29.5	102.7
3	50.0	137.3	50.0	143.3	50.0	138.0	50.0	132.8	50.0	107.7	50.0	83.6

Points 1, 2 and 3 defined in Eq. (50). For EE1 (only M) has also a point at 2/3 M_{jrd}, i.e., at 3.5-mrad rotation and 90.0-kN m bending moment.

Table 9
Comparisons between the experimental and the proposed model initial stiffness and the experimental and the proposed model design moment.

Tests	Initial stiffness (kN m/rad)				Design moment (kN m)			
	Model	Exp	Mod/Exp	%	Model	Exp	Mod/Exp	%
EC 3 (only M)	24,055	23,467	1.03	−3	121	119	1.02	−2
EE1 (only M)	25,785	23,467	1.10	−10	135	119	1.14	−14
EE2 (+10% N_{pl})	13,445	13,554	0.99	1	128	125	1.02	−2
EE3 (+20% N_{pl})	12,885	13,169	0.98	2	120	118	1.02	−2
EE4 (+27% N_{pl})	12,369	12,538	0.99	1	112	113	0.99	1
EE6 (−10% N_{pl})	9,771	9,274	1.05	−5	118	116	1.02	−2
EE7 (−20% N_{pl})	7,317	6,829	1.07	−7	103	101	1.02	−2

Negative percentage means overestimated value of X% whilst positive percentage indicates underestimated value of X%. Joint design moment is determined according to Eurocode 3 [4], through the intersection between two straight lines, one parallel with the initial stiffness and another parallel with the moment–rotation curve post-limit stiffness.

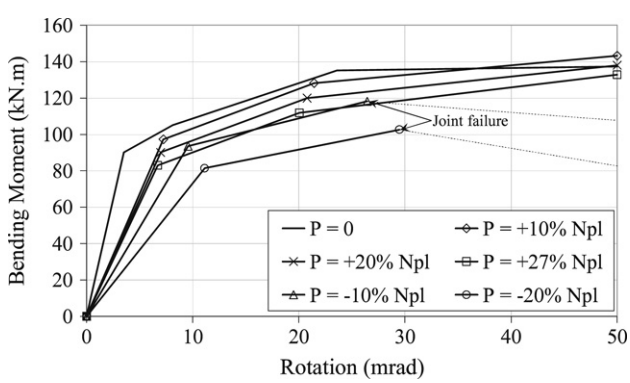

Fig. 21. Prediction of six moment–rotation curves for different axial force levels.

of 10% and 20% of the beam axial plastic resistance. For these last two cases the joint plasticity was governed by yielding of the endplate in bending, followed by yielding of the beam bottom flange in compression. An accurate prediction of the initial stiffness and flexural capacity are observed, Table 9. However, as the tensile force increases to 20% of the beam axial plastic resistance, a slight difference is exhibited overestimating the initial stiffness by 7%, Fig. 20(f). For both cases of tensile forces evaluated by the proposed mechanical model, the joint failures before reaching a 0.05-rad rotation.

Fig. 21 illustrates the set of numerical results where it is possible to observe that the extended endplate joint subjected both to compressive and tensile forces has its initial stiffness and flexural capacity decreased as either compressive or tensile force increases. This reduction in the initial stiffness is more pronounced for tensile forces applied to the joint. Additionally it is worth highlighting that the joint initial stiffness is strongly influenced by the rigid link lever arm d. Joints possessing similar rigid link lever arms d exhibited a small variation of the initial stiffness as can be seen on the compressive force numerical results, Fig. 21: $P = +10\% N_{pl}$, $P = +20\% N_{pl}$ and $P = +27\% N_{pl}$.

Generally the global behaviour of the numerical moment–rotation curves, obtained by using the generalised mechanical model proposed in this work, is in agreement with the test curves, Lima et al. [11], producing numerical results that closely approximate the initial stiffness and flexural resistance, Table 9. These small discrepancies might be attributed to the simplifications made in the generalised mechanical model as well as possible inaccuracies in the assumed material and geometrical properties.

5. Conclusions

Based on the general principles of the component method, a generalised mechanical model was proposed to estimate the endplate joint behaviour when both bending moments and axial forces are present. This mechanical model is able to deal with three basic requirements for the joint performance: strength, stiffness and deformation capacity. Application and validation of this mechanical model, using experimental tests executed by Lima et al. [11] on six extended endplate joints, was performed and led to accurate prediction of the experiment's key variables.

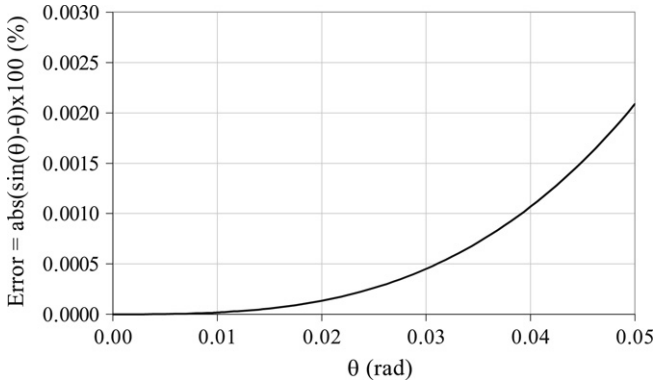

Fig. 22. First-order approximations error magnitudes versus joint rotation.

The utilization of this generalised mechanical model is simple and provides an approach to estimate the bending moment versus rotation curve for any axial force level. The tri-linear characterisation of the joint components suggested in this work was shown to be capable of reasonable approximations for the moment–rotation curve construction. However, further experimental examination and numerical analysis using different ranges of joints to check the validity and application of the proposed strain hardening coefficients, Table 2, beyond the scope of joints studied in this work is desirable.

The approach proposed for evaluation of lever arm *d*, Section 2.4, takes into account the change of the joint compressive centre according to the axial force levels and bending moment applied to the joint. This strategy was responsible for a satisfactory estimation for the joint initial stiffness, even before yielding of the first weakest component was reached.

First order approximations for the trigonometric expressions were used throughout the generalised mechanical model formulation. In this way, Fig. 22 presents the error due to these approximations versus joint rotations. According to Nethercot & Zandonini [13], rotations beyond 0.05 rad have little practical significance. This rotation was assumed as being the joint final rotation. For this value it is possible to observe in Fig. 22 an error of 0.002%. This indicated that the developed equations are accurate for the usual problems involving beam-to-column joints.

Some topics requiring further research have been identified in the process of developing and applying the proposed mechanical model. These include extension of the model to composite joints; to prove mathematically if the suggested lever arm position evaluation accurately represents the variations in the joint compressive centre position as a function of the joint loads; and further experimental investigations associated with a wider range of axial force magnitudes and different joint layouts.

Acknowledgements

The authors gratefully acknowledge the financial support provided by the Brazilian National and State Scientific and Technological Developing Agencies: CNPq, CAPES and FAPERJ. This arrangement financed the first author's period as a visiting scholar at Imperial College London.

References

[1] SCI Publication 183. Design of semi-continuous braced frames-specialist design guides. The Steel Construction Institute; 1997.
[2] Ramli-Sulong NH, Elghazouli AY, Izzuddin BA. Behaviour and design of beam-to-column connections under fire conditions. Fire Safety Journal 2007; doi:10.1016/j.firesaf.2006.09.003.
[3] Vlassis AG, Izzuddin BA, Elghazouli AY, Nethercot DA. Design oriented approach for progressive collapse assessment of steel framed buildings. Structural engineering international (report). SEI Editorial Board; 2006. p. 129–36.
[4] Eurocode 3: Design of steel structures – Part 1.8: Design of joints. Brussels: European Committee for Standardisation; May 2005.
[5] Li TQ, Choo BS, Nethercot DA. Connection element method for the analysis of semi-rigid frames. Journal Constructional Steel Research 1995;32:143–71.
[6] Nethercot DA. Steel beam to column connections: A review of test data and their application to the evaluation of joint behaviour on the performance of steel frames. CIRIA Project Record 338. London; 1985.
[7] Weynand K. SERICON I—Databank on joints building frames. In: Proceedings of the 1st COST C1 workshop. 1992. p. 28–30.
[8] Cruz PJS, Simões da Silva LAP, Rodrigues DS, Simões RAD. SERICON II—Database for the semi-rigid behaviour of beam-to-column connections in seismic regions. Journal of Constructional Steel Research 1998;46(1–3): 233–234.
[9] Guisse S, Vandegans D, Jaspart J-P. Application of the component method to column bases — Experimentation and development of a mechanical model for characterization. Report no. MT 195, Liege: Research Centre of the Belgian Metalworking Industry; 1996.
[10] Wald F, Svarc M. Experimental with endplate joints subject to moment and normal force. Contribution to experimental investigation of engineering materials and structures. CTU Report n: 2–3. Prague; 2001. p. 1–13.
[11] Lima LRO, de Simoes da Silva L, Vellasco PCGS, de Andrade SA. Experimental evaluation of extended end-plate beam-to-column joints subjected to bending and axial force. Engineering Structures 2004;26:1333–47.
[12] Simões da Silva L, de Lima LRO, Vellasco PCGS, de Andrade SA. Behaviour of flush end-plate beam-to-column joints under bending and axial force. Steel and Composite Structures 2004;4(2):77–94.
[13] Nethercot DA, Zandonini R. Methods of prediction of joint behaviour: Beam-to-column connections. In: Structural connections: Stability and strength. London and New York: Elsevier Applied Science; 1989. p. 23–62 [Chapter 2].
[14] Baker JF. Second report, London: Steel Structures Research Committee, Department of Scientific and Industrial Research. HMSO; 1934.
[15] Rathbun J. Elastic properties of riveted connections. Transactions on American Society of Civil Engineers 1936;101:524–63.
[16] Lionberger SR, Weaver W. Dynamics response of frames with non-rigid connections. Journal of Engineering Mechanical Division, ASCE 1969;95(EM1): 95–114.
[17] Romstad KM, Subramanian CV. Analysis of frames with partial connection rigidity. ASCE, Journal of Structural Division 1970;96(ST11):2283–300.
[18] Kennedy DJL. Moment–rotation characteristics of shear connections. Engineering Journal, American Institute of Steel Construction 1969;(October): 105–15.
[19] Sommer WH. Behaviour of welded header plate connections. Master's thesis. Ontario (Canada): University of Toronto; 1969.
[20] Frye MJ, Morris GA. Analysis of flexibility connected steel frames. Canadian Journal of Civil Engineering 1975;2:280–91.
[21] Ang KM, Morris GA. Analysis of 3-dimensional frames with flexible beam-column connections. Canadian Journal of Civil Engineering 1984;11:245–54.
[22] Ramberg W, Osgood WR. Description of stress–strain curves by 3 parameters. Technical Report 902. National Advisory Committee for Aeronautics; 1943.
[23] Moncarz PD, Gerstle KH. Steel frames with nonlinear connections. Journal of Structural Division, ASCE 1981;107(ST8):1427–41.
[24] Poggi C, Zandonini R. Behaviour and strength of steel frames with semi-rigid connections. In: Chen WF, editor. Connection flexibility and steel frame behaviour. American Society of Civil Engineers; 1985.
[25] Jones SW, Kirby PA, Nethercot DA. Modelling of semi-rigid connection behaviour and its influence on steel column behaviour. In: Howlett JH, et al., editors. Joints in structural steelwork. London: Pentech Press; 1981. p. 573–87.
[26] Lui EM, Chen WF. Analysis and behaviour of flexibly jointed frames. Engineering Structures 1986;8(2):107–15.
[27] Nethercot DA, Kirby PA, Rifai AM. Design of columns in PR construction: Analytical studies. Canadian Journal of Civil Engineering 1987;14(4):485–97.
[28] Yee KL, Melchers RE. Moment–rotation curves for bolted connections. ASCE, Journal of Structural Engineering 1986;112(3):615–35.
[29] Kishi N, Chen WF, Matsuoka KG, Nomachi SG. Moment–rotation relation of top- and seat-angle with double web-angle connections. In: Bjorhovde R, et al., editors. Connections in steel structures: Behaviour, strength and design. London: Elsevier Applied Science Publishers; 1988. p. 121–34.
[30] Kishi N, Chen WF, Matsuoka KG, Nomachi SG. Moment–rotation relation of single/double web-angle connections. In: Bjorhovde R, editor. Connections in steel structures: Behaviour, strength and design. London: Elsevier Applied Science Publishers; 1988. p. 135–49.
[31] Chen WF, Kishi N. Moment–rotation relation of top and seat angle connections. Report CE-STR-87-4. Department of Structural Engineering, Purdue University; 1987. p. 16.
[32] Richard RM, Gillett PE, Kriegh JD, Lewis BA. The analysis and design of single plate framing connections. Engineering Journal of American Institute of Steel Construction 1980;17(2):38–52.
[33] Richard RM, Abbott BJ. Versatile elastic–plastic stress–strain formula. ASCE, Journal of Engineering Mechanical Division 1975;101(EM4):511–5.

[34] Altman WG, Azizinamini A, Bardburn JH, Radziminski JB. Moment–rotation characteristics of semi-rigid steel beam-column connections. Civil Engineering Department, University of South Carolina; 1982.
[35] Mazzolani FM. Mathematical model for semi-rigid joints under cyclic loads. In: Bjorhovde R, et al., editors. Connections in steel structures: Behaviour, strength and design. London: Elsevier Applied Science Publisher; 1988. p. 112–20.
[36] Del Savio AA, Nethercot DA, Vellasco PCGS, Andrade SA, Martha LF. Developments in semi-rigid joint moment versus rotation curves to incorporate the axial versus moment interaction. In: Third international conference on steel and composite structures. 2007b. p. 1–7.
[37] Lewitt CW, Chesson E, Munse W. Restraint characteristics of flexible riveted and bolted beam to column connections. Bulletin no. 500. Chicago: Engineering Experiment Station, University of Illinois; 1969.
[38] Johnson RP, Law CLC. Semi-rigid joints for composite frames. In: Howlett JH, editor. Joints in structural steelwork. London: Pentech Press; 1981. p. 33–319.
[39] Richard RM, Hsia WK, Chmielowiec M. Derived moment rotation curves for double framing angles. Computers and Structures 1988;30(3):485–94.
[40] Elsati MK, Richard RM. Derived moment rotation curves for partially restrained connections. Structural Engineering Review 1996;8(2–3):151–8.
[41] Wu FH, Chen WF. A design model for semi-rigid connections. Engineering Structures 1990;12:88–97.
[42] Kishi N, Chen WF. Moment–rotation of semi-rigid connections with angles. Journal of Structural Engineering, ASCE 1990;116(7):1813–34.
[43] Foley CM, Vinnakota S. Toward design office moment–rotation curves for end plate beam-to-column connections. Journal of Constructional Steel Research 1994;217–53.
[44] Faella C, Piluso V, Rizzano G. Structural steel semi-rigid connections: Theory, design and software. CRC Press LLC; 2000.
[45] Bose SK, McNeice GM, Sherbourne AN. Column webs in steel beam to column connections. Part I, Formulation and verification. Computers and Structures 1972;2:253–72.
[46] Lipson SL, Hague MI. Elasto-plastic analysis of single-angle bolted-welded connections using the finite element method. Computers and Structures 1978; 9(6):533–45.
[47] Krishnamurthy N, Huang HT, Jeffrey PK, Avery LK. Analytical moment–rotation curves for end-plate connections. ASCE, Journal of Structural Division 1979; 105(ST1):133–45.
[48] Richard RM, Rabern DA, Hornby DE, Williams GC. Analytical models for steel connections. In: Hall WJ, Gaus MP, editors. Behaviour of metal structures (Proc. W. H. Munse symposium, May). American Society of Civil Engineers; 1983.
[49] Patel KV, Chen WF. Nonlinear analysis of steel moment connections. ASCE, Journal of Structural Engineering 1984;110(8):1861–75.
[50] Patel KV, Chen WF. Analysis of a fully bolted moment connection using NONSAP. Computers and Structures 1985;21(3):505–11.
[51] Kukreti AR, Murray TM, Abolmaali A. End-plate connection moment–rotation relationship. Journal of Constructional Steel Research 1987;8:137–57.
[52] Beaulieu D, Picard A. Finite element modelling of connections. In: Bjorhovde R, et al., editors. Connections in steel structures: Behaviour, strength and design. London: Elsevier Applied Science Publishers; 1988. p. 96–103.
[53] Atamiaz Sibai W, Frey F. Numerical simulation of the behaviour up to collapse of two welded unstiffened one-side flange connections. In: Bjorhovde R, et al., editors. Connections in steel structures: Behaviour, strength and design. London: Elsevier Applied Science Publishers; 1988. p. 85–92.
[54] Sherbourne AN, Bahaari MR. 3D simulation of end-plate bolted connections. Journal of Structural Engineering, ASCE 1994;120(11):3122–36.
[55] Bursi OS, Jaspart J-P. Benchmarks for finite element modelling of bolted steel connections. Journal of Constructional Steel Research 1997;43(1–3):17–42.
[56] Bursi OS, Jaspart J-P. Calibration of a finite element model for isolated bolted end-plate steel connections. Journal of Constructional Steel Research 1998; 44(3):225–62.
[57] Yang JG, Murray TM, Plaut RH. Three-dimensional finite element analysis of double angle connections under tension and shear. Journal of Constructional Steel Research 2000;54:227–44.
[58] de Cardoso DCL. Numerical modelling of semi-rigid connection for steel structures. Ph.D. thesis. Rio de Janeiro (Brazil): PUC-Rio, Pontifical Catholic University, Civil Eng. Dept.; 2001 [in Portuguese].
[59] Citipitioglu AM, Haj-Ali RM, White DW. Refined 3D finite element modelling of partially-restrained connections including slip. Journal of Constructional Steel Research 2002;58:995–1013.
[60] Coelho AG, Bijlaard F, Simoes da Silva L. On the behaviour of bolted end plate connections modelled by welded T-stubs. In: European conference on steel structures—Eurosteel 2002. p. 907–18.
[61] Maggi YI, Goncalves RM, Malite M. Comparative analysis of bolted T-stub and corresponding extended endplate connections: A numerical approach. In: European conference on steel structures. Eurosteel 2002. p. 1199–218.
[62] Wales MW, Rossow EC. Coupled moment-axial force behaviour in bolted joints. ASCE, Journal of Structural Engineering 1983;109(5):1250–66.
[63] Kennedy DJR, Hafez M. A study of end-plate connections for steel beams. Canadian Journal of Civil Engineering 1984;11(2):139–49.
[64] Chmielowiec M, Richard RM. Moment rotation curves for partially restrained steel connections. Report to AISC. University of Arizona; 1987. p. 127.
[65] Tschemmernegg F. On the nonlinear behaviour of joints in steel frames. In: Bjorhovde R, et al., editors. Connections in steel structures: Behaviour, strength and design. London: Elsevier Applied Science Publishers; 1988. p. 158–65.
[66] Tschemmernegg F, Humer C. The design of structural steel frames under consideration of the non-linear behaviour of joints. Journal of Constructional Steel Research 1988;11:73–103.
[67] Madas JP. Advanced modelling of composite frames subjected to earthquake loading. Ph.D. thesis. Imperial College Science, Technology and Medicine, University of London; 1993.
[68] Finet L. Influence de l'effort normal sur le calcul des assemblages semi-rigides. Diploma work. Clermont-Ferrand (France): CUST; July 1994 [in French].
[69] Jaspart J-P, Braham M, Cerfontaine F. Strength of joints subjected to combined action of bending moments and axial forces. In: European conference on steel structures—Eurosteel 1999. p. 465–8.
[70] Cerfontaine F. Etude de l'interaction entre moment de flexion et effort normal dans les assemblages boulonnés. Doctor en Sciences appliquées – Université de Liege, Faculté des Sciences Appliquées; 2003 [in French].
[71] da L Nunes PC. Parametrical analysis of structural steel endplate joints subjected to bending moment and axial force. M.Sc. dissertation. Rio de Janeiro (Brazil): PUC-Rio, Pontifical Catholic University, Civil Eng. Dept.; 2006 [in Portuguese].
[72] de Lima LRO. Behaviour of endplate beam-to-column joints under bending and axial force. Ph.D. thesis. Rio de Janeiro (Brazil): PUC-Rio, Pontifical Catholic University, Civil Eng. Dept.; 2003 [in Portuguese].
[73] Pucinotti R. Top-and-seat and web angle connections: Prediction via mechanical model. Journal of Constructional Steel Research 2001;57:661–94.
[74] Eurocode 3. Annex J: Joints in building frames. ENV 1993-1-1:1992/A2. Brussels: European Committee for Standardisation; 1998.
[75] Simões da Silva L, Coelho AMG. An analytical evaluation of the response of steel joints under bending and axial force. Computers & Structures 2001;79: 873–81.
[76] Sokol Z, Wald F, Delabre V, Muzeau J-P, Svarc M. Design of endplate joints subject to moment and normal force. In: Third European conference on steel structures—Eurosteel 2002. Coimbra: Cmm Press; 2002. p. 1219–28.
[77] Ramli-Sulong NH. Behaviour of steel connections under fire conditions. Ph.D. thesis. Imperial College London, University of London; 2005.
[78] Urbonas K, Daniunas A. Behaviour of semi-rigid steel beam-to-beam joints under bending and axial forces. Journal of Constructional Steel Research 2006; 62:1244–9.
[79] Simões da Silva L, Santiago A, Vila Real P. Post-limit stiffness and ductility of end-plate beam-to-column steel joints. Computers & Structures 2002; 80(5–6):515–31.
[80] Kuhlmann U, Davison JB, Kattner M. Structural systems and rotation capacity. In: Proceeding of COST conference on control of the semi-rigid behaviour of civil engineering structural connections. 1998. p. 167–76.
[81] Del Savio AA, Nethercot DA, Vellasco PCGS, Andrade SA, Martha LF. A component method model for semi-rigid end-plate beam-to-column joints including the axial versus bending moment interaction. In: Fifth international conference on advances in steel structures. 2007. p. 1–6.